PALEOENVIRONMENTAL ANALYSIS IN COASTAL SYSTEMS

DEVELOPING NEW PALEOENVIRONMENTAL APPROACHES FOR CARIBBEAN COASTAL SYSTEMS - CASE STUDIES FROM PUNTA DE CARTAS AND PLAYA BAILEN, CUBA, AND LITTLE SALT SPRING, FLORIDA

By

Braden Ross Buchanan Gregory, B.Sc.

A Thesis

Submitted to the School of Graduate Studies

In Partial Fulfilment of the Requirements

For the Degree

Master of Science

McMaster University

MASTER OF SCIENCE (2014) McMaster University
(Geography and Earth Sciences) Hamilton, Ontario, Canada

TITLE: Developing new paleoenvironmental approaches for Caribbean coastal systems - case studies from Punta de Cartas and Playa Bailen, Cuba, and Little Salt Spring, Florida

AUTHOR: Braden R.B. Gregory, B.Sc.
(McMaster University, Hamilton, Ontario, Canada, 2004)

SUPERVISOR Professor Eduard G. Reinhardt

NUMBER OF PAGES: x, 67 pp.

ABSTRACT

Tropical latitudes play an important role in global climate as they export moisture and energy pole-ward. Recent tests of predictive climate models against Holocene paleoclimate data show discrepancies between predicted and observed values in tropical regions. Terrestrial paleoclimate records could help resolve these discrepancies by all allowing for better understand of the sensitive ocean-atmosphere climate dynamics in the tropics and by providing additional information from a diverse source of proxies.

The Caribbean is an ideal location for study as its climate is influenced by both the Atlantic and Pacific Oceans. However, there are relatively few terrestrial basins that contain paleoclimate proxies due to the archipelagic nature of the region. If Caribbean climate is to be thoroughly investigated, additional environments and climate proxies need to be investigated.

As coastal systems are ubiquitous throughout the Caribbean, they are ideal for investigation of Holocene paleoclimate in this region. However, they can be ephemeral on millennial timescales making them challenging to use in paleoclimate analysis. This dissertation discusses new methods and basins that facilitate the study of these systems. Several important contributions have been made by this thesis. (1) Core scanning XRF data, when examined with additional proxies such as foraminifera, can be used to infer shifts in regional precipitation patterns in a coastal setting. Though these methods have been used before in deep basins, this represents the first use of core scanning XRF in a littoral setting. (2) The evolution of sinkhole sedimentation is reliant on both the morphology of the sinkhole and water level within the feature.

ACKNOWLEDGEMENTS

First I would like to thank Dr E.G. Reinhardt, my supervisor, who has offered my encourage and direction throughout my graduate and undergraduate career. Thank you Ed, for introducing me to the joys of micropaleontology, coffee and quality safety razors.

I must also thank Dr. Matthew Peros of Bishop's University and Dr. John A. Gifford of the University of Miami, both of whom were integral to this project. Dr. Peros provided samples and trace element data for Cuba and environmental analysis would have no been what it was without his inputs. Thank you also for including me in additional Cuban projects whose funding kept me eating meat on a weekly basis. Dr. J.A. Gifford was kind enough to allow me to work on cores he had taken in the early 90s and provided insight into the archaeological history of Little Salt Spring which aided analysis greatly. Thank you both sincerely.

To my committee members, Dr. Joe Boyce and Dr. Francine McCarthy, thank you for taking the time to look over this thesis. I hope the rushed nature of this thesis was not too much of an inconvenience for either of you and I greatly appreciate your accommodation of my schedule.

Thanks go out to the members of the members of the McMaster Group for Stable Isotopologues, particularly Martin Knyf who helped with all stages of isotope analysis from preparation to calibration of results.

Thanks are also extended to my colleagues in the Geology department at McMaster. To my lab mates, Shawn Collins and Shawn Kovacs, who assisted me in many endeavours in the lab and the field, thank you. To my office-mates from GSB 301, thanks for your encouragement over the years and the many distractions you offered; I may not have remained sane without them Thank you also to my family and friends, whom helped me many times with either a beer, or a warm meal. Finally, an extra special thanks to Holleh Rahmati, who put up with me throughout this degree.

TABLE OF CONTENTS

LIST OF FIGURES

All figures are located at the end of their respective chapters, in consecutive order.

CHAPTER 2

the miniature blue graphs which show the calibrated distribution of ages for a given date. Dates with a black "X" through them were removed before generation of the age model to minimize age reversals.

Figure 3.4: Grain size sample statistics (mean, mode, standard deviation) alongside interpolated PSD plot for LSS core IV. The grey ribbon on mean grain size represents the within-sample standard deviation and the black line represents sample mean value. The x-axis of the PSD represent grain size (ϕ), the y-axis represents depth in core and the z-axis, represented with color, indicates % volume of sediment. Warmer colours (pink, red) indicate higher volume % of sediment. See identification key for a visual description of how to interpret PSD plots.

Figure 3.5: Summary diagram of mean grainsize, LOI and geochemical data for LSS Core IV. The grey ribbon on the mean grain size data represents within-sample standard deviation in ϕ. Data is divided into different phases using black lines with corresponding phases shown on the right.

Figure 3.6: Sea level curves and coral growth data for the Caribbean. Data points on the graph are reproduced from the corrected dataset of Milne and Peros (2013). Crosses represent peat deposits with vertical bars representing the range of sea level for each sample point and the horizontal bars representing age related error. Inverted "T"s represent coral sea level points with the lower limit representing minimum sea level and horizontal bars representing age related error.

Figure 3.7: Depositional model for LSS. Dashed and solid lines represent water level in the sinkhole at the start and end of each phase respectively. See discussion for further details.

LIST OF TABLES

All tables are located at the end of their respective chapters, in consecutive order.

CHAPTER 2

CHAPTER 3

CHAPTER 1

1.1 INTRODUCTION

Thermally induced circulation and upper tropospheric planetary scale waves (Rossby waves) transport energy and precipitation from the equatorial regions to mid and upper latitudes (Rasmusson and Wallace, 1983, Heaviside and Czaja, 2013, Stenseth et al., 2003). Through these teleconnections, tropical convection, controlled by local sea surface temperature (SST) and regional SST gradients, can influence global climate (Chiang et al., 2009). El Nino/the Southern Oscillation (ENSO), a SST and sea level pressure oscillation in the equatorial Pacific, has been correlated to warmer temperatures in Southeastern Africa and South western Canada, decreased incidence of hurricanes in the Atlantic Ocean, and decreased Caribbean precipitation (Ropelewski and Halpert, 1987, Rasmusson and Wallace, 1983, Donnelly and Woodruff, 2007, Giannini et al., 2001, Donders et al., 2005). Similarly, the expansion of the Atlantic Warm Pool, an area of $>28.5^{0}$C surface water in the Gulf of Mexico, has recently been correlated to decreased precipitation in central America, increased precipitation in the northern Caribbean and higher hurricane intensity (Wang et al., 2006, Donders et al., 2009). As well, changes in the position of the inter-tropic convergence zone (ITCZ), a zone of high convection controlled by the gradient between north and south Atlantic SST (Chiang et al., 2009) can alter precipitation in subtropical regions (Haug et al., 2001, de Mahiques et al., 2009, Donders et al., 2011, Shinn et al., 2006).

Despite the apparent influence tropical systems have on global climate, uncertainty remains as to how they will respond in the near future (Collins et al., 2010). Comparisons of modelled and paleoclimate data still contain discrepancies associated with poorly simulated or misrepresented ocean-atmosphere feedbacks (Otto-Bliesner et al., 2009, Braconnot et al., 2012). Additional terrestrial climate data from the tropics could offer insight into how regional oceanic and atmospheric climate oscillations influence tropical climate ultimately increasing the accuracy of present day models and their predictive ability. Climate in the Caribbean has been correlated to changes in both Pacific and Atlantic Oceans (Donnelly and Woodruff, 2007, Toomey et al., 2013, Haug et al., 2001, Hodell et al., 1995, Enfield and Alfaro, 1999, Giannini et al., 2001) making it an ideal location to study the influence of ocean-atmosphere dynamics on terrestrial climate in the tropics.

Any geomorphic feature that collects sediment for an extended period of time can retain paleoclimate data. Lakes are a common source of data in terrestrial systems as they remain relatively stable over millennial timescales, act as regional sediment sinks and preserve a wealth of environmental proxies such as microorganisms, pollen, and geochemical tracers (Grimm et al., 2006, Peros et al.,

2006, Hodell et al., 1995, Curtis et al., 1996, among others). Unfortunately, the islands of the Caribbean contain relatively few deep lakes, necessitating the use of other sources of paleoclimate information. The archipelagic nature of Caribbean yields itself to a prominence of coastal environments. Coastal systems offer many features that can preserve biological and geological signals (Leorri et al., 2006, Peros et al., 2006, Culver, 2013, Donnelly et al., 2007, Lui and Fearn., 2000, McCloskey and Keller., 2009). However, the ephemeral nature of coastal environments can cloud environmental interpretations (Lane et al., 2011). Although this problem has been solved in the past through the use of multiple proxies, these methods are time intensive hindering the efficiency of paleoclimate analysis in these systems. If Caribbean coastal systems are to be a viable source of paleoclimate data, new methods and more stable environments need to be considered for paleoclimate analysis.

Developing additional methods for quickly gathering data from coastal sediments would both encourage the use of coastal systems in paleoclimate analysis, and improve the efficacy of their paleoenvironmental reconstructions. Core Scanning X-Ray Fluorescence (XRF) is a relatively new technique that produces qualitative trace element data (Lowenmark et al., 2010). This method has been used to extract paleoclimate data from offshore sedimentary records in deep basins (Haug et al., 2001, Montero-Serrano et al., 2010, Toomey et al., 2013) and on continental shelves (de Mahiques et al., 2009, Kujua et al., 2010, Lamy et al., 2001, Bertrand et al., 2007). These systems are relatively stable and any change in trace element composition therefore reflects changes in trace element inputs, which can be used to infer provenance of sediment (Yao et al., 2012, Haug et al., 2001, Betrand et al., 2007, Montero-Serrano et al., 2010, Kujau et al., 2010). If a coastal basin remains relatively stable over time, sediments would record similar environmental proxy data. In Chapter 2, we explore the combined use of foraminifera and XRF data as a source of paleoclimate information in coastal systems.

If uncertainties associated with the ephemeral morphology of coastal systems can be circumvented, they will become a more viable source of paleoclimate information. A recent solution to this issue has been the use of karstic basins for paleoclimate data. Karstic environments are ubiquitous throughout the Caribbean and offer a variety of features that act as sediment sinks such as sinkholes, blueholes and aquatic caves. These basins remain stable after their formation and may record sediment from periods of much lower sea level as many sinkholes are be exceedingly deep (Brown et al., 2013, Shinn et al., 1996, Gischler et al.,2008, 2013). Despite these advantages, karstic basins remain relatively unexplored in terms of environment and sedimentology. Recently, sediments from sinkholes have been used to examine hurricane incidence (Brown et al., 2013, Gischler et al., 2008, Lane et al., 2010), sea level rise (Gabriel et al., 2011) and precipitation trends (Alvarez-Zarikian et al., 2005, Bernhardt et al.,

2010, 2012) during the Holocene. However, issues with redeposition and reworking of sediment (Kovacs et al., 2013) and only limited environmental and sedimentological data (van Hengstum et al., 2011, Schmitter-Soto et al., 2002) in these environments hinders their use as a paleoclimate archive. Chapter 3 explores the controls on sedimentation in a sinkhole on the coast of Florida in order to further develop the understanding of these environments for future use in the paleoclimate analysis of coastal systems.

1.2 RESEARCH OBJECTIVES

The main research objective of this dissertation is to increase the viability of using coastal environments for paleoclimate research through the application of the relatively new techniques and by providing insight into the depositional regime of karst basins through the examination of sinkhole sedimentology. More specifically, this dissertation addresses the questions:

(1) Is XRF a viable source of paleoclimate information in a littoral setting when combined with additional proxies, such as foraminifera?

(2) What are the major controls on sedimentation within sinkholes?

1.3 DISSERTATION STRUCTURE

This thesis represents a compilation of two papers addressing the aforementioned research questions. In Chapter 2, sediments taken from two lagoons in Cuba are examined for paleoclimate information using XRF, foraminifera, and lithology of sediments. Variations in absolute amount of Ti, Fe, and K in sediment corroborate foraminifera evidence which indicates Cuba underwent alternating periods of wet and dry conditions during the last 4,000 yr BP. Chapter 3 examines the sedimentology of Little Salt Spring, a sinkhole 20 km inland from the west coast of Florida. Isotopic, grain size and lithologic data indicates that both rising water table and the morphology of sinkhole controlled sedimentation patterns. It was also revealed that organic portion in sinkholes may provide evidence of climate change and stable periods in sinkhole deposition more strongly reflect these changes. Although a possible climate signal is recorded in the grain size for part of the LSS record, the absence of this signal during other periods of deposition emphasizes the caution that must be taken when interpreting paleoclimate information from sinkholes.

REFERENCES

Alvarez-Zarikian, C.A., Swart, P.K., Gifford, J.A. and Blackwelder, P.L. (2005).

Holocene paleohydrology of Little Salt Spring, Florida, based on ostracod assemblages and stable isotopes. *Palaeogeography, Paleoclimatology, Palaeoecology,* 225, 134-156.

Bernhardt, C.E., Willard, D., Landacre, B. and Gifford, J. (2010). Vegetation changes during the last deglacial and early Holocene: a record from Little Salt Spring,Florida (Abstract #PP41B-1635). *Proceedings from AGU '10: The American Geophysical Union Fall Meeting,* San Francisco, CA.

Bernhardt, C.E., Willard, D.A. and Gifford, J. (2012). Pollen evidence for a cool, dry Younger Dryas and warm, wet Early Holocene in the southeastern United States. *Proceedings from the IPC '12: the 13th International Palyno logical Congress,* Tokyo, Japan.

Bertrand, S., Hughen, K., Pantoka, S., Sepulveda, J. and Lange, C. (2007). Late Holocene climate variability of Northern Patagonia reconstructed by a multi-proxy analysis of Chilean fjord sediments (44-47°S). *Geophysical Research Abstracts,* 9.

Braconnot, P., Harrison, S.P., Kageyama, M., Bartlein, P.J., Masson-Delmotte, V., Abe-Ouchi, A., Otto-Bliesner, B. and Zhao, Y. (2012). Evaluation of cliamte models using palaeoclimatic data. *Nature Climate Change,* 2, 417-424.

Brown, A., Reinhardt, E.G., van Hengstum, P.J. and Pilarcyzk, J.E. (2013). A coastal Yucatan sinkhole records intense hurricane events. *Journal of Coastal Research,* 294, 418-428.

Chiang, J.C.H. (2009). The Tropics in Paleoclimate. *Annu. Rev. Earth Planet. Sci.,* 37, 263 - 297. Collins, M., An, S.-I., Cia, W., Ganachaud, A., Guilyardi, E., Jin, F.-F., Jochum, M., Lengaige, M., Power, S. Timmermann, A., Vecchi, G. and Wittenberg, A. (2010). The impact of global warming on the tropical Pacific Ocean and El Niño. *Nature Geoscience,* 3, 391-396.

Culver, S.J. (2013). Benthic foraminifera of Puerto Rican mangrove-lagoon systems: Potential for paleoenvironmental interpretation. *PALAIOS,* 5, 34-51.

Curtis, J., Hodell, D. and Brenner, M. (1996). Climate variability on the Yucatan Peninsula (mexico) during the past 3500 years, and implications for Maya cultural evolution. *Quaternary Research,* 47, 37-47.

Donders, T.H., Wagner, F., Dilcher, D.L. and Visscher, H. (2005). Mid- to late-Holocene El Niño-Southern Oscillation dynamics reflected in the subtropical terrestrial realm. *Proceedings of the National Academy of Sciences of the United States of America,* 102, 10904-10908

Donnelly, J.P. and Woodruff, J.D. (2007). Intense hurricane activity over the past 5000 years controlled by El Nino and the West African monsoon. *Nature,* 447, 465-468.

Enfield, D.B. and Alfaro, E.J. (1999). The dependence of Caribbean rainfall on the interaction of the Tropical Atlantic and Pacific Oceans. *Journal of Climate,* 12, 2093-2103.

Gabriel, J.J., Reinhardt, E.G., Peros, M.C., Davidson, D.E., van Hengstum, P.J. and Beddows, P.A. (2008). Palaeoenvironmental evolution of Cenote Aktun Ha (Carwash) on the Yucatan Peninsula, Mexico, and its response to Holocene sea-level rise. *Journal of Paleolimnology,* 42, 199-213.

Giannini, A., Chiang, J.C.H., Cane, M.A., Kushnir, Y. and Seager, R. (2001). The ENSO teleconnection to the Tropical Atlantic Ocean: Contributions of the remote and local SSTs to rainfall variability in the Tropical Americas. *Journal of Climate,* 14, 4530-4544.

Gischler, E., Shinn, E.A., Oschmann, W., Fiebig, J. and Buster, N.A. (2008). A 1500-year Holocene Caribbean climate archive from the Blue Hole, Lighthouse Reef, Belize. *Journal of Coastal Research,* 246, 1495-1505.

Grimm, E.C., Watts, W.A., Jacobson, G.L., Hansen, B.C.S., Almquist, H.R. and Dieffenbacher-Krall, A.C. (2006). Evidence of warm wet Heinrich events in Florida. *Quaternary Science Reviews,* 25, 2197-2211.

Haug, G.H., Hughen, K.A., Sigman, D.M., Peterson, L.C. and Röhl, U. (2001). Southward migration of the intertropical convergence zone through the Holocene. *Science,* 293, 1304 - 1308.

Heaviside, C. and Czaja, A. (2013). Deconstructing the Hadley cell heat transport. *Quarterly Journal of the Royal Meteorological Society,* 139, 2181-2189.

Hodell, D.A., Curtis, J.H. and Brenner, M. (1995). Possible role of climate in teh collapse of Classic Maya civilization. *Letters to Nature,* 375, 391-394.

Kujau, A., Nürnberg, D., Zielhofer, C., Bahr, A. and Röhl, U. (2010). Mississippi River discharge over the last ~560,000 years - Indications from X-ray fluorescence core-scanning. *Palaeogeography, Paleoclimatology, Palaeoecology,* 298, 311-318.

Kovacs, S.E., van Hengstum, P.J., Reinhardt, E.G., Donnelly, J.P. Albury, N.A. (2013). Late Holocene sedimentation and hydrologic development in a shallow coastal sinkhole on Great Abaco Island, The Bahamas. *Quaternary International,* 317, 118-132.

Lamy, F., Hebbeln, D., Röhl, U. and Wefer, G. (2001). Holocene rainfall variability in southern Chile: a marine record of latitudinal shifts of the Southern Westerlies. *Earth and Planetary Science Letters,* 185, 369-382.

Lane, P., Donnelly, J. Woodruff, J.D. and Hawkes, A.D. (2011). A decadelly-resolved paleohurricane record archived in the late Holocene sediments of a Florida sinkhole. *Marine Geology,* 287, 14-30.

Lee, J.-Y., Wang, B., Sea, K.-H., Kug, J.-S., Choi, Y.-S., Kosaka, Y. and Ha, K.-J. (2014). Future change of the northern hemisphere summer Tropical-Extratropical teleconnections in CMIP5 models. *Journal of Climate,* 27, 3643-3664.

Leorri, E., Martin, R. and McLaughlin, P. (2006). Holocene environmental and parasequence development of the St. Jones Estuary, Delaware (USA): Foraminiferal proxies of natural climatic and anthropogenic change. *Palaeogeography, Paleoclimatology, Palaeoecology,* 241, 590-607.

Liu, K. and Fern, M.L. (2000). Reconstruction of prehistoric landfall frequencies of catastrophic hurricanes in northwestern Florida from lake sediment records. *Quaternary Research,* 54, 238-245.

Lowenmark, L. Chen, H.F., Yang, T.N., Kylander, M., Yu, E.F., Hsu, Y.W., Lee, T.Q., Song, S.R. and Jarvis, S. (2011). Normalizing XRF-scanner data: A cautionary note on the interpretation of high resolution records from organic-rich lakes. *Journal of Asian Earth Sciences,* 40, 1250-1256.

Mahiques, M.M., Wainer, I.K.C., Burone, L., Nagai, R., Sousa, S.H.M., Figueira, R.C.L., Silveira, I.C.A., Bicego, M.C., Alves, D.P.V. and Hammer, O. (2009). A high-resolution Holocene record on the Southern Brazilian shelf: Paleoenvironmental implications. *Quaternary International,* 206, 52-61.

McCloskey, T.A. and Keller, G. (2009). 500 year sedimentary record of hurricane strikes on the central coast of Belize. *Quaternary International,* 195, 53-68.

Montero-Serrano, J.C., Bout-Roumazeilles, V., Sionneau, T., Tribovillard, N., Bory, A., Flower, B.P., Riboulleau, A., Martinez, P. and Billy, I. (2010). Changes in precipitation regimes over North America during the Holocene as recorded by mineralogy geochemistry of Gulf of Mexico sediments. *Global and Planetary Change,* 74, 132-143.

Otto-Bliesner, B.L., Schneider, R., Brady, E.C., Kucera, M., Abe-Ouchi, A., Bard, E., Braconnot, P., Crucifix, M., Hewitt, C.D., Kageyama, M., Marti, O., Paul, Rosell-Melé, A., Waelbroeck, C., Weber, S.L., Weinelt, M. and Yu, Y. (2009). A comparison of PMIP2 model simulations and the MARGO proxy reconstruction for tropical sea surface temperatures at last glacial maximum. *Climate Dynamics,* 32, 799-815.

Peros, M.C., Reinhardt, E.G. and Davis, A.M. (2007). A 6000-year record of ecological and hydrological changes from Laguna de la Leche, north coastal Cuba. *Quaternary Research,* 67, 69-82.

Rasmusson, J. and Wallace, E. (1983). Meteorological aspects of El Niño/Southern Oscillation. *Science,* 222, 1195-1202.

Ropelewski, C. and Halpert, M. (1987). Global and regional scale precipitation patterns associated with the El Niño/Southern Oscillation. *Monthly Weather Review,* 115, 1606-1626.

Schmitter-Soto, J.J., Comín, F.A., Escobar-Briones, E., Alcocer, H.-S.J., Suárez-Morales, E., Elías-Gutierrez, M., Díaz-Arce, V., Marín, L.E. and Steinich, B. (2002). Hydrogeochemical and biological characteristics of cenotes in the Yucatan Peninsula (SE Mexico). *Hydrobiologia,* 467, 215-228.

Shin, S.-I. Sardeshmukh, P.D. and Webb, R.S. (2006). Understanding the Mid-Holocene Climate. *Journal of Climate,* 19, 2801-2817.

Stenseth, N., Ottersen, G., Hurrell, J.W., Mysterud, A., Lima, M., Chan, K.-S., Yoccoz, N.G. and Ådlandsvik, B. (2003). Studying climate effects on ecology through the use of climate indices: The north Atlantic Oscillation,

El Niño Southern Oscillation and beyond. *Proceedings: Biological Sciences,* 270, 2087-2096.

van Hengstum, P.J., Scott, D.B., Gröcke, D.R. and Charette, M.A. (2011). Sea level controls sedimentation and environments in ocastal caves and sinkholes. *Marine Geology,* 286, 35-50.

Wang, C., Enfield, D.B., Lee, S.-K. and Landsea, C.W. (2006). Influences of the Atlantic Warm Pool on Western Hemisphere summer rainfall and Atlantic hurricanes. *Journal of Climate,* 19, 3011-3028.

Yao, Z., Liu, Y., Shi, X and Suk, B.C. (2012). Paleoenvironmental changes in the East/Japan Sea during the last 48 ka: indications from high-resolution X-ray fluorescence core scanning. *Journal of Quaternary Science,* 27, 932-940

CHAPTER 2

FORAMINIFERAL AND XRF ELEMENTAL ANALYSIS OF TWO CUBAN LAGOONS DOCUMENT INCREASED ARIDITY DURING THE MID-LATE HOLOCENE

Braden R.B. Gregory, Matthew Peros, Eduard G. Reinhardt

2.1 ABSTRACT

Coastal lagoons are not often used as paleoclimate archives because of their complex geomorphic history which can be affected by climate and sea-level change. This study from Punta de Cartas and Playa Bailen, Cuba shows that combined foraminiferal and XRF elemental analysis can isolate the effects of climate change (wet vs dry) on lagoon environments. Foraminiferal assemblages from both Punta de Cartas and Playa Bailen show increasing diversity over the past 4000 yrs BP with a prominent increase at ~1100-1400 yrs BP. Assemblages were initially dominated by *Ammonia* spp. (eg. *Ammonia tepida*) and *Elphidium* spp. (eg. *Elphidium excavatum*) indicating brackish salinity but increasing minor species, such as miliolids (eg. *Triloculina* spp. *Quinqueloculina* spp.), indicate a shift to more marine conditions up-core. Correspondingly, terrigenous input into the lagoon (Fe, Ti and K) generally declined over the past 4000 yrs BP but showed a flexion point at ~1100-1200 yrs BP likely due to decreasing precipitation. Fe, Ti and K have been used as proxies for weathering rates in tropical and sub-tropical basins with greater input during wet vs dry periods but have never been applied to shallower lagoon systems with their complex geomorphic histories. The shared timing between the XRF and foraminiferal data inferring decreased freshwater input into the lagoon provides confidence for the onset of drier climate conditions. The correspondence between the two lagoons situated ~ 10 kms apart suggests a regional effect with increasingly arid conditions developing since the mid-Holocene (4 ka) but with a pronounced trend over the last ~ 1200 yrs BP which matches other climate records from the Caribbean.

2.2 INTRODUCTION

The study of Caribbean climate during the Holocene is of increasing interest due to its influence on northern latitudes (teleconnections; Chiang et al., 2009). In the last decade many studies have focused on climate archives in Belize (Gischler and Storz, 2009, McCloskey and Keller, 2009), Jamaica (Holmes et al., 1995), Haiti (Hodell et al, 1991, Higuera-Gundy et al., 1999), Venezuela (Haug et al 2001, 2003, Black et al., 2004), Puerto Rico, St Martin (Malaize et al., 2011), Grenada (Fritz et al., 2011) and the Yucatan (Medina-Elizalde et al., 2010, Frappier et al., 2014). However, paleoclimate information from Cuba is limited

with only speleothem $\delta^{18}O$ records by Fensterer et al. (2013) and palynological, microfossil and isotope work by Peros et al. (2007a, b). More data is needed to constrain Holocene climate change both temporally and spatially in the Caribbean but there few suitable deep lakes for study. Although speleothem records have provided an excellent data source (Fensterer et al., 2013, Mangini et al., 2007), the lack of diversity in paleoclimate records can hinder reconstructions as proxies respond differentially to climate forcing and a multitude of spatial and temporal records are needed for informative reconstructions. Accurate reconstructions of environmental systems are vital for testing climate models and examining the importance of climate feedbacks (Masson-Delmonte et al., 2006, Sloan and Barron, 1992, Braconnot et al., 2012). Recent analysis by the Paleoclimate Modeling Intercomparison Project showed relatively poor agreement between modeled and observed tropical sea surface temperatures emphasizing the need for investigation of climate feedbacks in tropical regions (Braconnot et al., 2012). There is also little information on how Cuban lagoons will respond to future climate perturbations and their often fragile ecosystems.

Coastal environments, such as estuaries and lagoons aren't often used for paleoclimate records as uncertainty in the geomorphic evolution of the environment can pose difficulties for reconstructing climate signals. The study of estuaries and lagoons often relies on paleosalinity proxies for understanding the effects of sea-level rise and barrier configuration and there are several reliable paleosalinity indicators for coastal environments which are often combined (eg. paleontologic and geochemical analysis; Peros et al., 2007). Foraminifera and ostracods have been used extensively for reconstructing paleo-environmental evolution of estuaries and lagoons as they respond predictably to salinity change. Within a given lagoon or estuary, salinity is a function of sea-level, barrier configuration and freshwater input due to changing precipitation and evaporation rates**. The multiple variables influencing salinity can make isolation of the primary cause of salinity shifts difficult** (Cheng et al., 2012, Peros et al., 2007, Cann and Cronin, 2004, Hodell et al, 2005, Gabriel et al., 2009, Cann et al., 2000, van Hengstum et a., 2010, Brewster-Wingaard and Ishman, 1999).

Trace elemental analysis of sediments has increased in application with the development of high resolution X-Ray Fluorescence (XRF) core scanning in the early 2000s that measures the bulk trace elemental composition of the sediments (Haug et al., 2001, Lamy et al., 2001). The trace elemental composition of sediments is a combination of deposited mineral material, solutes in the water scavenged by organic flocculants and clays, and biotic and abiotic precipitates from the water (eg. calcareous and silicious shells and tests) which can be affected by early diagenesis such as redox migrations of elements in the upper sediments (Battiston et al., 1993). Many different mineral combinations have been used to indicate a wide range of factors affecting depositional processes which can be environment or basin specific (Thanachit et al., 2006, Rothwell et

al., 2006, Thomson et al., 2006). Fe, Ti, and K have been used to indicate increased weathering of continental rocks and alluvium within the drainage basin (Thanachit et al., 2006). Increased precipitation can intensify weathering and transportation of terrigenous elements towards the basinal depocenter via runoff (eg. Haug et al., 2001, Lamy et al., 2001). The relationship between precipitation and terrigenous sediment input has been established in many environments including deep ocean basins (Haug et al., 2001, Mora and Martinez, 2005, Yao et al., 2012., Yarincik et al., 2000), continental shelves and slopes (Arz et al., 1998, Lamy et al., 2001, Zabel et al., 2001, de Mahiques et al., 2009) and lacustrine areas (Bertrand et al., 2005, Haberzettl et al., 2008, Warrier and Shankar, 2009, Lowenmark et al., 2010, Saez et al., 2009). Though as yet applied to lagoon sediments, similar relationships should apply assuming the lagoon acts as a sediment sink and is closed or semi-closed relative to the larger basin.

Here we present high resolution XRF data in conjunction with foraminifera results from two lagoons in Cuba (Punta de Cartas and Playa Bailen). The foraminiferal data documents salinity shifts over the past 4000 years while the trace elements (Fe, Ti and K) show changes in weathering patterns. Comparisons between the two datasets allows isolation of precipitation and its influence on lagoon salinity which shows similarities between the two locations suggesting a regional response. Understanding the role of precipitation in the evolution of coastal lagoons and ponds will be useful for understanding climatic response and anthropogenic impacts through economic development in other Caribbean locations.

2.3 STUDY AREA

Two lagoons on the south-western coast of Cuba were analyzed (Fig. 2.1). Punta de Cartas is an elliptical shaped, restricted lagoon found on the northern shore of the Bahia de Cortez. Punta de Cartas exists as the seaward extent of a larger wetland system composed of dense red mangrove *(Rhizophora mangle)* forests and shallow ponds. A ~100 m barrier of developing mangrove, beach grasses and sand separates the lagoon from the ocean. Presently, a 200m long, 5m wide channel intersects this barrier connecting the lagoon to the ocean.

Playa Bailen is located on the western shore of the Bahia de Cortez 15km south west of Punta de Cartas. Unlike Punta de Cartas, Playa Bailen is topographically isolated from the surrounding wetlands to the North and West. Playa Bailen is elongated parallel to the shoreline (NE – SW). A ~100m barrier separates Playa Bailen from the ocean. Presently, this barrier supports a small community and public beach which has altered its natural condition. Swaths of red mangrove fringe Playa Bailen encroaching into the lagoon and there are small stands of mangrove in the open water areas.

Punta de Cartas and Playa Bailen are on the sheltered shoreline of Bahia de Cortez which is part of the westernmost extent of Cuba's continental shelf which extends 15 km offshore. North of the lagoons is a shallow coastal plain 10 – 15 km wide comprising of alluvium from the southern terranes of the Los Organos mountain range further to the north (Itrualde-vincent, 1994). The mountainous terranes are composed of Lower Jurassic siliclastic, coastal and shallow marine sediments overlain by Oxfordian shallow water conglomerates and carbonate platform sequences; incalations of tholeiitic basalt occur throughout these sequences and chert rich limestones of Oxfordian age (Itruald-vincent, 1994).

Climate in Pinar del Rio has an average temperature between 24-26°C (Neuvo Atlas Nacional de Cuba, 1989) and a summer wet season from May – October with a winter dry conditions from November – April. The southern coast of Pinar del Rio receives 1200 – 1400 mm of rainfall a year, ~1000 mm of which falls during the wet season. The wet season precipitation is distinctly bimodal with maximums occurring in June and August (**Neuvo Atlas Nacional de Cuba, 1989,** Seifriz, 1943).

2.4 METHODS

One core from each Punta de Cartas and Playa Bailen were collected with a Russian Peat Corer. Core PC01 was taken from Punta de Cartas at 22°10‘23.46“N, 83°49‘35.80“W and core PB02 was taken from Playa Bailen at 22°08’22.83 »N, 83°57’31.18“W (Fig. 2.1). Water depth at both coring sites was ~70cm at the time of sampling. A total of 275 cm of sediment was recovered at PC01 and 311 cm of sediments at PB02. Grey basal clay prevented further penetration at both locations.

Cores were analyzed for elemental composition and high resolution radiographic (XRI) and photographic images using an ITRAX core scanner at the Woods Hole Oceanagraphic Institution. Counts for 25 elements were recorded at 1 mm intervals for 20 s each interval using a Mo X-ray source. High resolution radiographic (XRI) and photographic images of PC01 and PB02 were recorded during the scanning process and used to document sedimentary structures and organic content.

Organic matter, silicate and carbonate content throughout the core were determined using loss on ignition (LOI) analysis following procedures outline by Dean (1974) and Heiri et al. (2001). Approximately $3cm^3$ of sediment was sampled at 1 cm intervals, weighed and dried in an overnight at 110°C. Once dry, samples were weighed and heated in a muffle furnace at 550°C for 4 hours, allowed to cool in a desiccator then re-weighed to provide estimates of Organic Matter (OM) content. Samples were then heated to 1000°C for two hours to

remove carbonates. Carbonate content ($CaCO_3$) was calculated with using the difference in weight between combustion steps divided by 0.44 which accounts for the proportion of CO_2 in $CaCO_3$ (Dean, 1974).

Foraminifera in cores PC01 and PB02 were examined at 10 cm intervals. Approximately 5 cm^3 of sediment was disaggregated and wet sieved at 63 microns to concentrate the foraminifera. Dry sediment was split and examined using a binocular dissecting microscope (YY-ZZ X Range of magnification) and foraminiferal identification followed that of Poag (1981) and Javaux and Scott (2004). Generally, 200 foraminifer were counted per sample as to ensure statistical significance of specimens (Patterson and Fishbein, 1989, Fatela and Tuborda, 2002). However, only a few dominant species were used as indicators of environmental change as their abundance clearly showed salinity trends. Standard error on species abundances (%) was calculated which determined confidence intervals (Patterson and Fishbein, 1989).

Stratigraphically constrained cluster analysis was conducted on samples using the R package Rioja (Juggins, 2012). Rioja uses the Constrained Increment Sum of Squares (CONISS) algorithm outlined in Grimm (1987). Number and position of biofacies within clusters were determined using a broken stick model generated by Rioja. The Shannon-Weaver Diversity Index (SDI) was used as a measure of diversity within samples, as diversity often changes with environment shifts (Murray, 1991, Culver, 1990). The SDI was calculated using the paleontological freeware program PAST. Summary figures where generated using Rioja and Analogue packages in R (Juggins 2012; Simpson and Oksanen, 2013).

Three samples of undifferentiated organic matter from both PB02 and PC01 were sent for AMS dating at Beta Analytic (Table 1). Dates were calibrated using the R package Clam (Blaauw, 2010) and the IntCal13.14C radiocarbon age calibration curve (Reimer et al., 2013). An additional implicit date of 0 yr BP was assumed for surface samples. **A smooth spline best approximated the observed dates and was therefore used in out age model**.

2.5 RESULTS

2.5.1 Lithology and LOI

2.5.1i Core PB02

PB02 is composed of mud with variable organic content ranging in colour from dark brown to grey mud. Intervals of elevated organic content are shown as brownish clays in RBG and darker grey in XRI images (Fig. 2.2). Images show thin horizontal bedding (<1 cm) throughout the core indicating little bioturbation. At the base of the core (310-330 cm), OM is generally low (<10%) but increases

between 230-310 cm to values that are higher and variable (~15-60 %). Between 0-230 cm OM values are lower (~10-15 %) but increase slightly (15-20%) between 0-80 cm. $CaCO_3$ values are higher but variable from 180-310 cm (~20-60 %) but drop sharply between 220-280 cm and have very low values (<10 %) relative to the rest of the core. In this same interval gypsum crystals several millimeters in length and columnar in habit are found. From 180 cm, $CaCO_3$ values gradually increase from 15 to 30 % towards the top of the core. The silicate fraction follows an inverse trend to that of the carbonates except between 220-280 cm where the OM content is high.

2.5.1ii Core PC01

Similarly to PB02, PC01 is composed of brown to grey mud due to variable amounts of OM (Fig. 2.3) with the XRI showing centimetre scale horizontal bedding with shifts in lithology closely following OM contents. The OM contents are generally low at < 5% from 210-275 cm but increase sharply to 7-9 % at 210 cm and then again at 70 cm reaching 25 % at the top of the core (Fig. 2.3). $CaCO_3$ is initially <5% but increases after 225 cm and becomes more variable (10-30 %) unto 170 cm. This is similar to that of PB02 except without the drop in values (220-280 cm). From 170 cm, $CaCO_3$ values are lower (~ 10%) and less variable but gradually increase to 15 % at the top of the core. The pattern of silicate values is an inverse of the $CaCO_3$ with a general decrease in values moving up-core.

2.5.2 X-Ray Fluorescence

Fe, Ti and K are reported in counts per second (cps) which only show relative changes in elements as errors associated with matrix and dilution effects prevent conversion to absolute values (Lowenmark et al., 2010). Fe is most abundant element in PC01 and PB02 peaking up to 45,000 cps but generally ranging from 5000 – 15,000 cps, Ti is less abundant between 100 and 1000 cps and K never exceeds 500 cps. In core PB02, Fe, Ti, and K correlate well with each other (r^2 >0.59) indicating all three elements are from the same source area. In core PC01, K and Fe have a strong positive correlation (r^2 > 0.50) but Ti is less (r^2 < 0.2992) which may indicate that Ti at Punta de Cartas may be coming from and an additional source. However, all three elements follow similar patterns in both cores suggesting regional scale processes affecting sedimentary input into the lagoons.

PB02 shows good agreement between K, Ti and Fe values (cps) except in the lower sections of the core (Fig. 2.2). Ti and K values (cps) decrease from 225 to 330 cm; Ti and K values are ~ 600 and 175 cps at the base to ~ 200 and 100 cps at 190 cm. In contrast, Fe values show an increase over this interval starting at ~ 500 and reaching 1000 cps at 225 cm, however, values are more consistent

through the rest of the core. Fe, Ti, and K are variable between 160 and 225 cm (26,523 - 1,174 cps; 762 - 25 cps; 345 - 24 cps) and gradually decrease after 160cm reaching very low values at the top of the core (Fe 2803 cps; Ti 64 cps; K 90 cps; Fig. 2.2).

Elemental concentrations at the base of core PC01 are high at 30,000, 800, and 250 cps respectively for Fe, Ti, and K (Fig 2.3) and gradually decrease to lower values at 190 cm. From 100 to 190 cm values are variable with several large peaks and lows (Fe 29,083 - 5,132 cps; Ti 1,024 - 47 cps; K 496 - 49 cps), and show a decreasing trend at 100 cm to the core-top (Fig. 2.3).

2.5.3 Foraminifera biofacies

2.5.3i Core PB02

Samples examined from core PB02 contained foraminifera at most depths excluding those between 220 – 270 cm and at 280cm (Fig 2.4). Foraminiferal species identified include *Elphidium excavatum, E. poeyanum, Ammonia beccari* forma *tepida, A. beccari* forma *pakinsoniana, Quinqueloculina seminulum, Q. Crassa, Q. Bosciana, Triloculina oblonga, T. Schreiberiana, Nionella atlantica, Furenskonia sp. Polymorphian sp.*, and *C. involvens*. Stratigraphically constrained cluster analysis separated foraminifera species into 4 distinct assemblages that follow an increasing marine tendency up core.

Assemblage 1 - the *Ammonia – Quinqueloculina* (AQ) Assemblage, is found from 280 – 330 cm. The AQ Assemblage is dominated by *A.beccari* forma *tepida* (27%), *Q. seminulum* (28%), *A. beccari* forma *parkinsoniana* (17%) and *Q. bosciana* (17%). Additional species of *Quinqueloculina*, *Triloculina* and *Elphidium* were present but were below ~10% on average. *Ammonia* species are tolerant of a range of salinity but both *Ammonia* and *Elphidium* species are normally found in brackish environments (Bradshaw, 1957, Labin, 1995, Debaney, 2000, Debaney and Guillou 2002, Hayward and Hollis 1994, Murray, 1991). *Quinqueloculina* and *Triloculina* are more commonly found in more marine salinities between 25 – 40 ppt but some species can be found in brackish-marine lagoons (Culver, 1990 Gischler et al., 2003, Debenay 2000, Debenay and Guillou, 2002, Hayward and Hollies, 1994, Murray, 1991, Wingaard and Ishman 1999). The Shannon Diversity Index (SDI) was moderate averaging 1.42. This species assemblage and diversity indicates polyhaline to euryhaline salinites likely between 25 but < 35 ppt.

Assemblage 2 - the Barren (B) Assemblage is composed of samples containing no foraminifera from 225 - 280 cm with the exception of 1 sample at 270 cm that contained minor amounts of *A. beccarri* forma *tepida*. *Ammonia* species, particularly *A. beccarri* forma *tepida*, are an opportunistic species capable

of tolerating abrupt salinity shifts and extreme salinities ranging from 1 – 90 ppt (Burone et al., 2012, Walton and Sloan, 1990, Labin, 1995). Gypsum crystals found in this interval may have been transported from lagoon margin areas, or may reflect stagnant and possibly anoxic bottom water conditions due to the degradation of OM content which is high during this period. This interval represents a period of harsh conditions not conducive to foraminifera colonization

Assemblage 3 - the *Ammonia* (A) assemblage consists of *Ammonia* species (*A. beccari* forma *tepida,* and forma *parkinsonniana*) with a combined average of ~55% but also contains *E. excavatum* and *Q. seminulum* (~10%) among other minor species. SDI values increase to an average of 1.74 is due to the increase in minor species, prominently *Triloculina* spp. and *N. atlantica*. These species are associated with marine salinities and shelf environments but can also be found in lagoon environments (Jarecki and Walkey, 2006, Culver, 1990, Gischler et al., 2003, Debaney 2000, Eichler et al., 2004, Hayward and Hollis, 1994). This indicates an overall increase in salinity from assemblage 1 and 2.

Assemblage 4 - the *Ammonia – Triloculina* Assemblage has similar diversity to the Assemblage 3 (average SDI 1.70). *Triloculina* spp, though initially lower, increase after 80 cm replacing *Ammonia* and *Quinqueloculina* as the dominant species. *Triloculina* species are associated with the upper range of marine values; notably *T. oblonga* has been associated with hypersaline conditions (Debaney et al., 2001, Murray 1991, Cheng et al., 2012). Other minor species (eg. *Fursenkonia sp.*) also increase in abundance during this interval indicating higher salinities closer to the normal marine salinity range (30-35 ppt) but maybe slightly higher (mixoeuhaline).

2.5.3ii Core PC01

A total of 12 foraminifera species were identified in PC01: *E. excavatum, E. poeyanum, Brizalina spathulata, A. beccari* forma *tepida, A. beccarri* forma *parkinsoniana, Furenskonia sp., N .atlantica,* and *Pyrgo* (Fig 2.5). CONISS cluster analysis revealed 3 assemblages and diversity was lower compared to PB02 (~1.5 vs 1.75) indicating slightly lower salinities overall, but showed a similar marine tendency moving up-core.

Assemblage 1 - is similar to the Barren Assemblage observed in PB02 in that foraminifera are generally very low or absent and the assemblage contains abundant *A. beccarri* forma *tepida* but also *Elphidium spp.* representing a brackish (polyhaline), possibly harsh environment as discussed previously. It ranges from 200-260 cm in the core (Fig 2.5).

Assemblage 2 and 3 - are most similar to the *Ammonia* Assemblage in PB02 and contain several other minor species whose abundance separates

Assemblage 2 and 3 (i.e. *N. atlantica, P. anomalas;* Figs. 2.5). Assemblage 2 ranges from 100-200 cm in the core and has comparatively lower diversity (1.25) than Assemblage 3. Assemblage 3 occurs from 0-100 cm has higher abundances of minor species and slightly increased SDI (1.39) representing a shift from brackish or polyhaline conditions (15- 30 ppt) to slightly more saline polyhaline conditions towards the core-top (25- 35 ppt; Figs. 2.5).

2.5.4 Chronology

The age model for PB02 shows an exponential increase in age up-core. Sediment accumulation rates average 1.1 mm/yr with higher rates at the top versus bottom of the core (Fig. 2.6). The error with the age model is approximately ± 100 yr BP. PC01's age model resembles an inverse cubic function with exponential age increase upto 110 cm and then a logarithmic age increase to the top of the core (Fig. 2.6). PC01 shows greater uncertainty in its age model than PB02 increasing from ±100 yr to ±125 yr after 50 cm. The rate of sediment accumulation in PC01 averages 0.86 mm/yr16.

2.6 DISCUSSION

2.6.1 Foraminifera and Salinity

The foraminifera data from Punta de Cartas and Playa Bailen show similar shifts in salinity during the Late Holocene though the actual assemblage found in each lagoon differ, Playa Bailen having a slightly higher diversity than Punta de Cartas, both locations show trends towards relatively more marine conditions spanning the last 3,000 - 4,000 yrs. Both locations show coeval transitions between assemblages - PB02 ~ 1100, 2300, and 3000 yrs BP; PC01 ~ 1400, and 2500 yrs BP suggesting a regional vs a basin specific effect.

At Playa Bailen, the *Ammonia-Quinqueloculina* Assemblage is found between 3000 and 4000 yr BP indicating polyhaline to euhaline salinities. The Barren Assemblage begins at ~3000 yr BP indicating harsher, perhaps anoxic, low salinity conditions which become slightly more marine ~2300 yr BP where the *Ammonia* Assemblage indicates polyhaline salinity. These conditions continue until ~1400 yr BP when the foraminiferal assemblage transitions to the higher diversity *Ammonia-Triloculina* assemblage indicating more marine salinities in the euhaline to metahaline range, which continued to present day.

Punta de Cartas shows a similar pattern. The Barren assemblage also occurs at Punta de Cartas albeit earlier than observed at Playa Bailen beginning at 3500 yr BP but terminates with similar timing to that of Playa Bailen at ~ 2500 yr BP. The relatively more marine *Ammonia* Assemblage is found in the lagoon

until 1500 yr BP when an increase in the concentration of minor species marks the shift to slightly more saline values in the upper range of polyhaline.

Laguna de Leche, located on the North Central coast of Cuba, shows similar salinity shifts as Playa Bailen and Punta de Cartas although the timing is slightly different which may be due to difficulties in radiocarbon dating the core from Laguna de Leche (approx. 1500 yr correction was applied to radiocarbon ages; Peros et al., 2007a,b). The transition from brackish to marine conditions was demarcated by the transition from an *Ammonia* biofacies to that containing *Elphidium spp.* and *Triloculina oblonga* which occurred after ~ 3200 yr BP although $^{87}Sr/^{86}Sr$ values show marine conditions in Laguna de Leche occurring after 2700 yr BP (Peros et al., 200??). In addition, palynological results showed an increase in *Chamaescyce,* an herb commonly found in dry salty soils, over the past 1400 years (Peros et al., 2007a,b).

This increasing marine tendency in Playa Bailen, Punta de Cartas and Laguna de Leche spanning the last 3500 yrs suggests regional scale forcing of salinity in Cuban lagoons (Fig. 2.7, Fig. 2.8).

2.6.2 Sediment, Sea-level and Lagoon Evolution

The cores in Playa Bailen, Punta de Cartas all met refusal on a grey clay at the base of the lagoons. Although no data was obtained from these deposits, the clay is likely from an earlier pond environment, which is a common feature in terrestrial areas of Caribbean Islands (eg. Pilarczyk et al., 2012) or may represent an intertidal mudflat environment which formed with initial sea-level rise flooding the terrestrial surface. Based on PB02 and PC01 the onset of marine influenced conditions occurred at least by 4000 yrs BP. Based on the water depth (~ 70 cm) and the core length at Play Bailen (330 cm) this corresponds with sea-level curves developed for the Caribbean (i.e. -2.75 to 3.5m at 4000 yr BP; Milne and Peros, 2013; Toscano and MacIntyre, 2005). The stratigraphic characteristics of PB02 and PC01 are relatively constant throughout the core suggesting sedimentation has kept pace with sea-level rise and water depth within the lagoons varied little during the observed record. The radiocarbon age model is consistent with constant sedimentation and the XRI data reinforces this interpretation as the sediments are bedded and undisturbed by bioturbation. There are trends in sediment composition (OM, $CaCO_3$, and silicates) but these tend to be fairly constant mostly varying by 10 - 20%.

This constant sedimentation, its muddy organic rich texture and the undisturbed bedding indicates that the barrier was emplace since at least 4000 yrs BP and likely formed not long after the transgression of sea-level to near its present location. The lack of any coarse sand intervals or any sedimentary structures in the cores suggests that the barrier has not been significantly modified

through its history. The foraminiferal data doesn't indicate any short-term changes in salinity associated with opening and closing of the barrier and the collective evidence indicates slowly rising sea-level with constant water depth (approx. 0.5-1 m) in an enclosed lagoon.

2.6.3 XRF data and Precipitation

The amount of terrigenous input, in this case inferred from Fe, Ti and K concentrations, has been used as a paleo-rainfall proxy in open marine basins but has never been applied to closed lagoonal systems (eg. Haug et al., 2001, others). Based on the previous discussion indicating relatively constant lagoon water depth and barrier morphology, precipitation should have a strong control on salinity within the lagoon.

Overall Ti shows the best relationship with the foraminifera and salinity reconstructions with an overall decreasing trend in values (cps) up-core in both Playa Bailen and Punta de Cartas. PB02 has Ti values at 400 cps at 4000 yr BP and 100 cps at the top of the core with a distinctive decline beginning at 1100-1200 yrs BP. PC01 shows a similar relationship with Ti values at 3500 yr BP (700 cps) decreasing to 200 cps at the core top with a flexion point at 1100-1200 yr BP. K and Fe values follow the same pattern in both cores.

There are matrix effects associated with core scanning XRF that may complicate elemental concentrations (Lowenmark et al., 2010). Notably, increases in organic content can significantly reduce cps resulting in erroneously low values. Crossplots of XRF data (Ti, Fe and K) show there is a weak negative relationship between trace elements and OM indicated by r^2 values below 0.1; Ti in core PC01 is an exception showing a slightly stronger relationship with OM (r^2 = 0.368) (Fig. 2.9). OM does increase (~ 10 to 20%) in the last ~ 1200 - 1400 years in both cores and this is also where Ti, Fe and K show a prominent decrease in cps values, but the magnitude of the change in OM and silicates is not concomitant with the change in elemental concentration (Fig. 2.7, 2.8). In the PB02 record there is a large increase in OM from 2300 - 3000 yr BP but has little effect on the elemental concentration (cps). The decrease in silicates or terrigenous input at ~ 1200 - 1400 years also would be expected with decreasing freshwater input into the lagoon.

The increase in salinity as recorded by the foraminifera and the decrease in Ti, Fe, and K indicate drier conditions with less freshwater discharge entering both Playa Bailen and Punta de Cartas since approximately 1200- 1400 yr BP.

2.6.4 Caribbean Precipitation trends.

The observed trend indicating higher salinity and decreased terrigenous input after ~ 1200 - 1400 years yr BP matches other paleoclimate proxies from the Caribbean which indicate the onset of more arid conditions during this time.

2.6.4i Coastal and Shelf Records

At Grand Case pond, St. Martin, an increase in evaporates occurred after 1100 yr BP and from 2350 - 4500 yr BP indicating drier conditions (Malaize et al., 2007). On the western coast of the Yucatan Peninsula, shifts in mangrove species indicate drier conditions occurring after 1,500 yr BP (Islebe and Sanchez, 2002). Pollen and geochemical data from a core taken in the back-barrier lagoon of Turneffe Atoll, Belize, imply an increasingly saline environment from 3,000 - 4,000 kyr BP and from 2,000 yr BP until the present, likely related to reduced precipitation (Wooller et al., 2009). The study which best correlates to the hypothesized climate trend is that of other XRF data from the Cariaco basin in the Southern Caribbean Sea (Haug et al., 2001). The amount of Ti and Fe in basin sediments decreases from 6,000 yr BP until the present indicative of a drier Late Holocene. This trend is interrupted by a plateau of relatively stable values from 1500 - 3500 yr BP after which values again decrease. The inflection point indicating increasingly dry conditions correlates with the Cuban trace element data enforcing the regional nature of this climate signal.

2.6.4ii Lacustrine Records

Lacustrine records also show evidence of increased aridity in the Late Holocene. Palynological and sedimentary evidence from crater lakes in Grenada indicate lower lakes levels from 1400 - 1600, and 600 - 1200 yr BP with increased aridity (Fritz et al., 2011). Oxygen isotopes from Lake Chichancanab in the central of the Yucatan Peninsula show a drying trend from 3,000 yr until the present with a period of intense dryness occurring from 1,500 - 1,000 yr BP followed by relatively stable, dry conditions (Hodell et al., 1995). At Lake Punta Laguna in the northeastern Yucatan Peninsula, a period of intense dry conditions (1,000 - 1,800 yr BP) was also observed in the oxygen isotope record, followed by a period of more stable, arid conditions (Curtis et al., 1996). Sedimentary records from a Lake Laguna Pallcacocha in Southern Ecuador also indicate a period of reduced precipitation from 1,800 - 2,300 yr BP bracketed by wetter conditions; the wet phases inferred from Laguna Pallcacocha represent evidence of El Niño/the Southern Oscillation (ENSO) events (Moy et al., 2002). ENSO has been correlated to drier conditions in the Caribbean (Giannini et al., 2001, Enfield and Alfaro, 1999) and is known to interfere with hurricane initiation in the Atlantic (Gray, 1984). Records from Puerto Rico to the south-east of Cuba show decreased intensity from 1000 yr to present correlating both with our precipitation data and the Ecuadorian El Nino record (Donnelly and Woodruff, 2007). Similarly, hurricane records from northwestern Florida show a period of hyperactivity from

~1,300 - 3,000 yr BP surrounding by periods of quiescence (Liu and Fern, 2000). These records suggest that precipitation and runoff in Cuba may be heavily dependent on Atlantic hurricane frequency.

2.7 CONCLUSION

The combined use of foraminifera and XRF elemental data allowed the isolation of both lagoon salinity and precipitation runoff allowing inferences to be made on climate patterns of Cuba in the Late Holocene. A clear increase in salinity and decrease in weathering inputs (Ti, Fe, K) at approximately ~ 1200 - 1400 years yr BP indicates the onset arid conditions in the Caribbean as shown in other studies. Subtle differences in the initiation of this aridity may be due to local influences, errors associated with dating, or differences in the environmental response to climate forcing across multiple proxies in terrestrial, littoral and marine realms. The correlation of paleoclimate records across the Caribbean with our trace element and foraminifera data suggest trends observed in Playa Bailen and Punta de Cartas are controlled by regional climate. Further study of other lagoons in Cuba will provide better confidence in this assessment.

This study demonstrates the applicability of trace element analysis using XRF core scanning to lagoon sediments. Coupling the elemental data showing terrigenous weathering flux with a paleosalinity proxy (eg. Foraminifera) can provide assessment of precipitation input and its effect on the lagoon basin. If the basin proven to be stable over time, via microfossil and stratigraphic data, XRF can produce useful paleoclimate data particularly in areas where other archives are not available.

2.8 REFERENCES

Arz, H.W., Pätzold, J. and Wefer, G. (1998). Correlated millennial-scale changes in surface hydrography and terrigenous sediment yield inferred from last-glacial marine deposits off north-eastern Brazil. *Quaternary Research,* 50, 157-166.

Battistion, G.A., Gerbasi, R., Degetto, S. and Sbrignadello, G. (1003). Heavy metal speciation in coastal sediments using total-reflection X-ray fluorescence spectromtry. *Spectrochimica Acta,* 48B, 217-221.

Bertrand, S., Hughen, K., Pantoja, S., Sepulveda, J. and Lange, C. (2007). Late Holocene climate variability of Northern Patagonia reconstructed by a multi-proxy analysis of Chilean fjord sediments (44-47^{o}S). *Geophysical Research Abstracts,* 9.

Black, D.E., Thunnell, R.C., Kaplan, A., Peterson, L.C. and Tappa, E.J. (2004). A 2000-year record of Caribbean and tropical North Atlantic hydrographic variability. *Paleoceanography,* 19, PA2022.

Blaauw, M. (2010). Methods and code for "classical" age-modelling of radiocarbon sequences. *Quaternary Geochronology,* 5, 1047-1059.

Braconnot, P., Harrison, S.P., Kageyama, M., Bartlein, P.J., Masson-Delmonte, V., Abe-Ouchi, A., Otto-Bliesener, B. and Zhao, Y. (2012). Evaluation of climate models using palaeoclimatic data. *Nature Climate Change,* 2, 417-424.

Brewster-Wingard, G.L. and Ishman, S.E. (1999). Historical trends in salinity and substrate in central Florida Bay: a paleoecological reconstruction using modern analogue data. *Estuaries,* 22, 369-383.

Burone, L/ Ortega, L., Franco-Fraguas, P., Mahiques, M., Garcia-Rodriguez, F., Vanturini, N., Marin, Y., Brugnoli, E., Nagai, R., Muniz, P., Bicego, M., Figueira, R. and Salaroli, A. (2013). A multiproxy study between the Rio de la Plata and the adjacent South-western Atlantic inner shelf to assess the sediment foorprint of river vs. marine influence. *Continental Shelf Research,* 55, 141-154.

Cann, J.H, Bouman, R.P and Bernett, E.J. (2000). Holocene foraminifera as indicators of relative estaurine-lagoonal and oceanic influences in estaurine sediments of the River Murray, South Australia. *Quaternary Research,* 53, 378-391.

Cann, J.H. and Cronin, T. (2004). An association of benthic foraminifera and gypsum in Holocene sediments of estaurine Chesapeake Bay, USA. *The Holocene,* 4, 614-620.

Cheng, J., Collins, L.S. and Holmes, C. (2012). Four thousand years of habitat change in Florida Bay as indicated by benthic foraminifera. *Journal of Foraminiferal Research,* 42, 3-17.

Chiang, J.C.H. (2009). The Tropics in Paleoclimate. *Annu. Rev. Earth Planet. Sci.,* 37, 263 - 297.

Culver, S. (1990). Benthic foraminifera of Puerto Rican mangrove-lagoon systems: potential for paleoenvironmental interpretations. *PALAIOS,* 5, 34-51.

Curtis, J.H., Hodell, D.A. and Brenner, M. (1996). Climate variability on the Yucatan Peninsula (Mexico) during the past 3500 years, and implications for Maya cultural evolution. *Quaternary Research,* 47, 37-47.

Dean, W.E. (1974). Determination of carbonate and organic matter in calcareous sediments and sedimentary rocks by loss on ignition: comparison with other methods. *Journal of Sedimentary Petrology,* 44, 242-248.

Debenay, J.P. (2000). Foraminifers of Paralic tropical environments. *Micropaleontology,* 46, 153-160.

Debenary, J.P., Geslin, E., Eichler, B.B., Duleba, W., Sylvestre, F. and Eichler, P. (2001). Foraminiferal assemblages in a hypersaline lagoon, Araruama (R.J.) Brazil. *Journal of Foraminiferal Research,* 31, 133-151.

Debenay, J.P. and Guillou, J.J. (2002). Ecological transitions indicated by foraminiferal assemblages in paralic environments. *Estuaries,* 25, 1107-1120.

Donnelly, J.P. and Woodruff, J.D. (2007). Intense hurricane activity over the past 5000 years controlled by El Nino and the West African monsoon. *Nature*, 447, 465-468.

Eichler, P.P.B., Castelão, G.P. , Pimenta, F.M., Eichler, B.B., de Miranda, L.B., Rodrigues, A.R. and Pereira, E.R.M. (2004). Foraminifera and thecamoebians as indicator of hydrodynamic process in a choked coastal lagoon, Laguna Estaurine System, SC, Brazil. *Journal of Coastal Research*, 39, 1144-1148.

Enfield, D.B. and Alfaro, E.J. (1999). The dependence of Caribbean rainfall on the interaction of the Tropical Atlantic and Pacific Oceans. *Journal of Climate*, 12, 2093-2103.

Fatela, F. and Taborda, R. (2002). Confidence limits of species proportions in microfossil assemblages. *Marine Micropaleontology*, 45, 169-174.

Fensterer, C., Scholz, D., Hoffman, D.L., Spötl, C., Schröder-Ritzrau, A., Horn, C., Pajón, J.M and Mangini, A. (2013). *Earth and Planetary Science Letters*, 361, 143-151.

Frappier, A.B., Pyburn, J., Pinkey-Drobnis, A.D., Wang, Xianfeng, Bornett, D.R., and Dahlin, B.H. (2014). Two millennia of tropical cyclone-induced mud layers in a northern Yucatán stalagmite reveal multiple overlapping climatic hazards during the Maya Terminal Classic 'megadroughts'. *Geophysical Research Letters*, in press.

Gabriel, J.J, Reinhardt, E.G., Peros, M.C., Davidson, D.E., van Hengstum, P.J. and Beddows, P.A. (2008). Palaeoenvironmental evolution of Cenote Aktun Ha(Carwash) on the Yucatan Peninsula, Mexico and its response to Holocene sea -level rise. *Journal of Paleolimnology*, 42, 199-213.

Giannini, A., Chiang, J.C.H., Cane, M.A., Kushnir, Y. and Seager, R. (2001). The ENSO teleconnection to the Tropical Atlantic Ocean: Contributions of the remote and local SSTs to rainfall variability in the Tropical Americas. *Journal of Climate*, 14, 4530-4544.

Gischler, E., Hauser, I., Heinrich, K. and Scheitel, U. (2003). Characterization of depositional environments in isolated carbonate platforms based on benthic foraminifera, Belize, Central America. *PALAIOS*, 18, 236-255.

Gischler, E. and Storz, D. (2009). High-resolution windows into Holocene climate using proxy data from Belize corals (Central America). *Palaeobio. Palaeoenv.*, 89, 211-221.

Gray, W.M. (1984). Atlantic seasonal hurricane frequency. Part 1: El nino and 30 mb quasi-biennial oscillation influences. *Monthly Weather Review*, 112, 1649-1668.

Grimm, E.C. (1987). CONISS: a FORTRAN 77 program for stratigraphically constrained cluster analysis by the method of incremental sum of squares. *Computer & Geosciences*, 13, 13-35.

Haberzettl, T., Kück, B., Wulf, S., Anselmetti, F., Arizetgui, D., Corbella, H., Fey, M., Janssen, S., Lücke, A., Mayr, C., Ohlendorf, C., Schábitz, F., Schleser, G.H., Wille, M. and Zolitschka, B. (2008). Hydrological

variability in southeastern Patagonia and explosive volcanic activity in the southern Andean Cordillera during Oxygen Isotope Stage 3 and the Holocene inferred from lake sediments of Laguna Potrok Aike, Argentina. *Palaeo3,* 259, 213-229.

Haug, G.H., Hughen, K.A., Sigman, D.M., Peterson, L.C. and Röhl, U. (2001). Southward migration of the intertropical convergence zone through the Holocene. *Science,* 293, 1304 - 1308.

Haug, G.H., Günther, D., Peterson, L.C., Sigman, D.M., Hughen, K.A. and Aeschlimann, B. (2003). Climate and the collapse of Maya civilization. *Science,* 299, 1731 - 1735.

Hayward, B. and Hollis, J. (1994). Brackish foraminifera in New Zealand: A taxonomic and ecologic review. *Micropaleontology,* 40, 185-222

Heiri, O., Lotter, A.F. and Lemcke, G. (2001). Loss on ignition as a method for estimating organic and carbonate content in sediments: reproducibility and comparability of results. *Journal of Paleolimnology,* 25, 101-110.

Higuera-Gundy, A., Brenner, M., Hodell, D.A., Curtis, J.H., Leyden, B.W., and Binford, M.W. (1999). A 10,300 ^{14}C yr record of climate and vegetation change from Haiti. *Quaternary Research,* 52, 159 - 170.

Hodell, D.A., Curtis, J.H., Jones, G.A., Higuera-Gundy, A., Brenner, M., Binford, M.W., and Dorsey, K.T. (1991). Reconstruction of Caribbean climate change over the past 10,500 years. *Letters to Nature,* 352, 790 - 793.

Hodell, D.A., Curtis, J.H. and Brenner, M. (1995). Possible role of climate in teh collapse of Classic Maya civilization. *Letters to Nature,* 375, 391-394.

Holmes, J.A., Street-Perrott, F.A., Ivanovich, M. and Perrott, R.A. (1995). A late Quaternary paleolimnological record from Jamaica based on trace-element chemistry of ostracod shells. *Chemical Geology,* 124, 143 - 160.

Islebe, G. and Sanchez, O. (2002). Hisotry of late Holocene vegetation at Quintana Roo, Caribbean coast of Mexico. *Plant Ecology,*160, 187-192.

Iturralde-Vincent, M.A. (1994). Cuban geology: a new plate-tectonic synthesis. *Journal of Petroleum Geology,* 17, 39-70.

Jarecki, L. and Walkey, M. (2006). Variable hydrology and salinity of salt ponds in the British Virgin Islands. *Saline Systems,* 2, 2.

Javaux, E. and Scott, D. (2003). Illustration of modern benthic foraminifera from Bermuda and remarks on distribution in other subtropical/tropical areas. *Palaeontologia Electronica,* 6, 1-29.

Juggins, S. (2012). Rioja: analysis of Quaternary science data. R package version 0.8-3. Retrieved from http://cran.2-project.org/package=rioja

Labin, A.A., Siman-Tov, R., Rosenfeld, A. and Debard, E. (1995). Occurrence and distribution of the foraminifer *Ammonia beccarii tepida* (Cushman) in water bodies, Recent and Quaternary, of the Dead Sea Rift, Israel. *Marine Micropaleontology,* 26, 153-159.

Lane, P., Donnelly, J. Woodruff, J.D. and Hawkes, A.D. (2011). A decadally-resolved paleohurricane record archived in the late Holocene sediments of a Florida sinkhole. *Marine Geology,* 287, 14-30.

Lamy, F., Hebbeln, D., Röhl, U. and Wefer, G. (2001). Holocene rainfall variability in southern Chile: a marine record of latitudinal shifts of the Southern Westerlies. *Earth and Planetary Science Letters,* 185, 369-382.

Liu, K. and Fearn, M.L. (2000). Reconstruction of prehistoric landfall frequencies of catastrophic hurricanes in northwestern Florida from lake sediment records. *Quaternary Research,* 54, 238-245.

Lowenmark, L. Chen, H.F., Yang, T.N., Kylander, M., Yu, E.F., Hsu, Y.W., Lee, T.Q., Song, S.R. and Jarvis, S. (2011). Normalizing XRF-scanner data: A cautionary note on the interpretation of high resolution records from organic-rich lakes. *Journal of Asian Earth Sciences,* 40, 1250-1256.

De Mahiques, M.M., wainer, I.K.C., Burone, L., Nagai, R., Sousa, S.H., Figueira, R.C.L., Silveira, I.C.A., Bicego, M.C., Alves, D.P.V. and Hammer, O. (2009). *Quaternary International,* 206, 52-61.

Mangini, A., Blumbach, P., Verdes, P, Spötl, C., Scholz, D., Machel, H. and Mahon, S. (2007). *Quaternary Science Reviews,* 26, 1332-1343.

Malaizé, B., Bertran, P., Carbonel, P., Bonnissent, D., Charlier, K., Galop, D., Imbert, D., Serrand, N., Stouvenot, C. and Pujol, C. (2011). Hurricanes and climate in the Caribbean during the past 3700 years BP. *The Holocene,* 21, 911-924.

Masson-Delmotte, V., Kageyama, M., Braconnot, P., Charbit, S., Krinner, G., Ritz, C., Guilyardi, E., Jouzel, J., Abe-Ouchi, A., Crucifix, M., Gladstone, R.M., Hewitt, C.D., Kitoh, A., LeGrande, A.N., Marti, O., Merkel, U., Motoi, T., Ohgaito, R., Otto-Bliesner, B., Peltier, W.R., Ross, I., Valdes, P.J., Vettoretti, G., Wber, S.L., Wolk, F. and Yu, Y. (2005). Past and future polar amplification of climate change: climate model intercomparisons and ice-core constraints. *Climate Dynamics,* 26, 513-529.

McCloskey, T.A., and Keller, G. (2009). 5000 year sedimentary record of hurricane strikes on the central coast of Belize. *Quaternary International,* 195, 53 - 68.

Medina-Elizalde, M., Burns, S.J., Lea, D.W., Asmerom, Y., Gunten, L.V., Polyal, V., Vuille, M. and Karmalkar, A. (2010)/ High resolution stalagmite climate record from the Yucatán Peninsula spanning the Maya terminal classic period. *Earth and Planetary Science Letters,* 298, 255-262.

Milne, G. and Peros, M.C. (2013). Data-model comparison of Holocene sea-level change in the circum-Caribbean region. *Global and Planetary Change,* 107, 119-131.

Mora, G. and Martinez, J. (2005). Sedimentary metal ratios in the Colombia Basin as indicators for water balance change in northern South America during the past 400,000 years. *Paleoceanography,* 20, PA4013.

Moy, C.M. Seltzer, G.O., Rodbell, D.T. and Anderson, D.M. (2002). Variability of El Niño/Southern Oscillation activity at millennial timescales during the Holocene epoch. *Nature,* 420, 162 - 165.

Patterson, T. and Fishbein, A. (1989). Re-examination of the statistical methods used to determine the number of point counts needed for micropaleontological quantitative research. *Journal of Paleontology*, 63, 245-248.

Peros, M.C., Reinhardt, E.G., Schwarcz, H.P. and Davis, A.M. (2007). High-resolution paleosalinity reconstruction from Laguna de la Leche, north coastal Cuba, using Sr, O, and C isotopes. *Palaeogeography, Palaeoclimatology, Palaeoecology* , 245, 535-550

Peros, M.C., Reinhardt, E.G. and Davis, A.M. (2007). A 6000-year record of ecological and hydrological changes from Laguna de la Leche, north coastal Cuba. *Quaternary Research*, 67, 69-82.

Pilarczyk, J.E. and Reinhardt, E.G. (2012). *Homotrema rubrum* (Lamarck) taphonomy as an overwash indicator in marine ponds on Anegada, British Virgin Islands. *Natural Hazards*, 63, 85-100.

Poag, C.W. (1981). Ecologic Atlas of Benthic Foraminifera, of the Gulf of Mexico. *Hutchinson Ross Publishing Company, Massachusetts, United States.*

Reimer, P.J., Bard, E., Bayliss, A., Beck, J.W., Blackwell, P.G., Bronk Rmasey, C., Buck, C.E., Edwards, R.L., Friedrich, M., Grootes, P.M., Guilderson, T.P., Haflidason, H., Hajdas, I., Hatté, C., Heaton, T.J., Hoffman, D.L., Hogg, A.G., Hughen, K.A., Kaiser, K.F., Kromer, B., Manning, S.W., Niu, M., Reimer, R.W., Richards, D.A., Scott, DE.M., Southon, J.R., Turney, C.S.M. and van der Plicht, J. (2013). IntCal13 and Marine13 radiocarbon age calibration curves, 0-50,000 years cal BP. *Radiocarbon,* 55, 1869-1887.

Rothwell, G.R., Hoogakker, B., Thomson, J., Croudace, I.W. and Frenz, M. (2006). Turbidite emplacement on the southern Balearic Abyssal Plain (western Mediterranean Sea) during Marine Isotope Stages 1-3: to lithostratigraphic analysis. In Rothwell, R.G. (Ed.), *New techniques in sediment core analysis,* (79-89). London: Geological Society of London Special Publications.

Sáez, A., Valero-Garcés, B.L., Giralt, S. Moreno, A., Bao, R., Pueyo, J.J., Hernández, A. and Casas, D. (2009). *Quaternary Science Reviews*, 28, 2743-2759.

Simpson, G.L. and Oksanen, J. (2013). Analogue: Analogue matching and modern analogue technique transfer function models. R package version 0.12-0. Retrieved from http://cran.r-project.org/package=analogue.

Seifriz, W. (1943). The Plant Life of Cuba. *Ecological Monographs*, 13, 375-426.

Sloan, L.C. and Barron, E.J. (1992). A comparison of Eocene climate model results to quantified paleoclimatic interpretations. *Paleo3*, 93, 183-202.

Thanachit, S., Suddhiprakarn, A., Kheorueromne, I. and Gikes, R.J. (2006). *Geoderma,* 135, 81-96.

Thompson, J., Croudace, I.W. and Rothwell, R.G. (2006). A geochemical application of the ITRAX scanner to a sediment core containing eastern Mediterranean sapropel units. In Rothwell, R.G. (Ed.), *New techniques in sediment core analysis,* (65-77). London: Geological Society of London Special Publications.

Toscano, M.A. and Macintyre, I.G. (2003). Corrected western Atlantic sea-level curve for the last 11,000 years based on calibrated ^{14}C dates from *Acropora palmata* framework and intertidal mangrove peat. *Coral Reefs,* 22, 257-270.

Van Hengstum, P.J., Reinhardt, E.G., Beddows, P.A., Gabriel, J.J. (2010)/ Linkages between Holocene paleoclimate and paleohydrogeology preserved in a Yucatan underwater cave. *Quaternary Science Reviews,* 29, 2788-2798.

Walton, W.R. and Sloan, B.J. (1990). The Genus *Ammonia* Brunnich, 1772: Its geographic distribution and morphologic variability. *Journal of Foraminiferal Research,* 20, 128-156.

Warrier, A. K. and Shankar, R. (2009). Geochemical evidence for the use of magnetic susceptibility as a paleorainfall proxy in the tropics. *Chemical Geology,* 265, 553-562.

Wooller, M.J., Behling, H., Guerrero, J.L., Jantz, N. and Zweigert, M.E. (2009). Late Holocene hydrologic and vegetation changes at Turneffe Atoll, Belize, compared with records from mainland Central America and Mexico. *PALAIOS,* 24, 650-656.

Yao, Z., Liu, Y., Shi, X and Suk, B.C. (2012). Paleoenvironmental changes in the East/Japan Sea during the last 48 ka: indications from high-resolution X-ray fluorescence core scanning.

Yarincik, K., Murrary, R. and Peterson, L.C. (2000). Climatically sensitive eolian and hemipelagic deposition in the Cariaco Basin, Venezuela, over the past 578,000 years: Results from Al/Ti and K/Al. *Paleoceanography,* 15, 210-228.

Zabel, M., Schneider, R.R., Wagner, T., Adegbie, A.T., Vreis, U and Kolonic, S. (2001). Late Quaternary climate changes in Central Africa, as inferred from terrigenous input to the Niger Fan. *Quaternary Research,* 56, 207-217.

CHAPTER 2 FIGURES

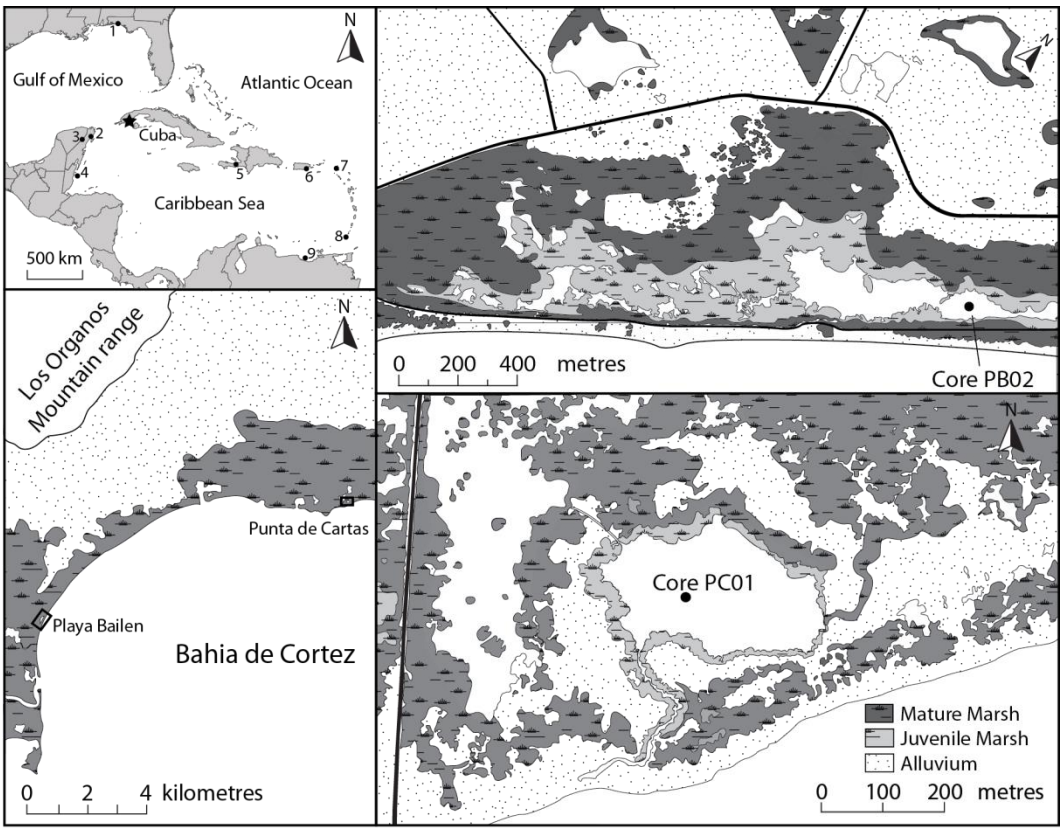

Figure 2.1: Map of the study areas. Top left: Location of the study areas and other climate records in the context of the Caribbean. Study sites are denoted by the black star. Other locations include (1) Western Lake, Florida (Liu and Fearn, 2000); (2) Puerto Morelos, Mexico (Islebe and Sánchez, 2002); (3) Lake Punta Laguna, Mexico (Curtis et al., 1996); (4) Turneffe Atoll, Belize (Wooller et al., 2009); (5) Lake Miragoane, Haiti (Hodell et al., 1995); (6) Laguna Playa Grande, Puerto Rico (Donnelly and Woodruff, 2007); (7) Grand Case Pond, St Martin (Malaize et al., 2011); (8) Lake Antoine, Grenada (Fritz et al., 2011); and (9) Cariaco Basin, Venezuela (Haug et al., 2001). Bottom left: Map of the area surrounding Punta de Cartas and Playa Bailen showing their relation to the Los Organos mountain range to the north and the Bahia de Cortez to the south. Top right: aerial view of Playa Bailen and the location of core PB02 as indicated by the black circle. Bottom right: Aerial view of Punta de Cartas with location of core PC01 shown by black circle.

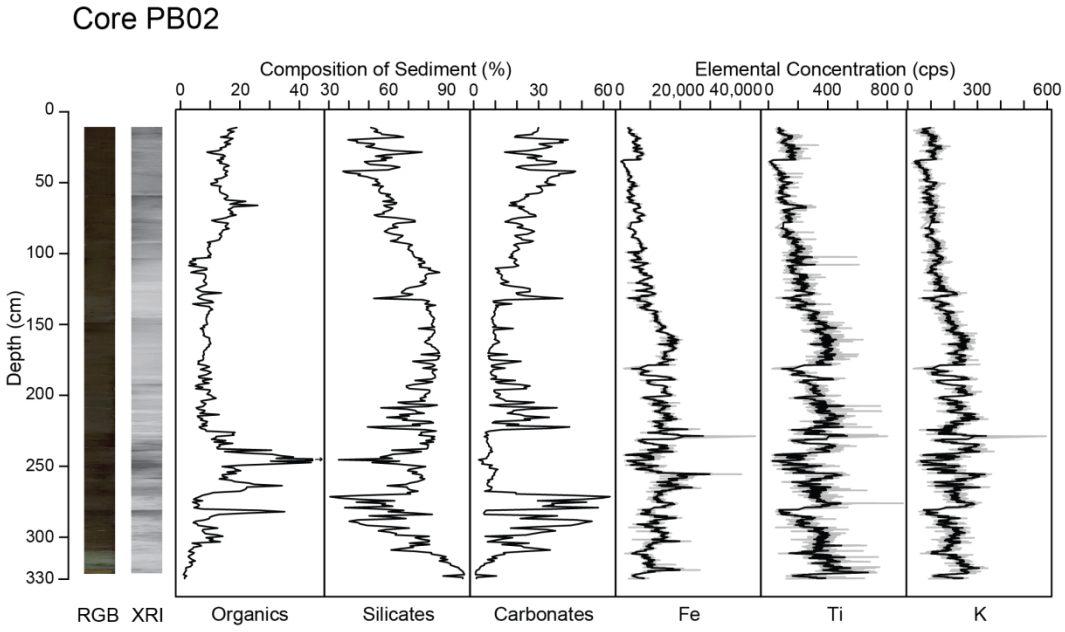

Figure 2.2: XRI and RGB images, LOI and trace element results from core PB02. From left to right: RBG and XRI images of the core, LOI results (organic content, silicates, and carbonates) reported in % of sediment composition, and the concentration of trace elements in the sediment as derived from core scanning XRF. The grey line represents raw XRF values while the black line represents the 5-point running mean.

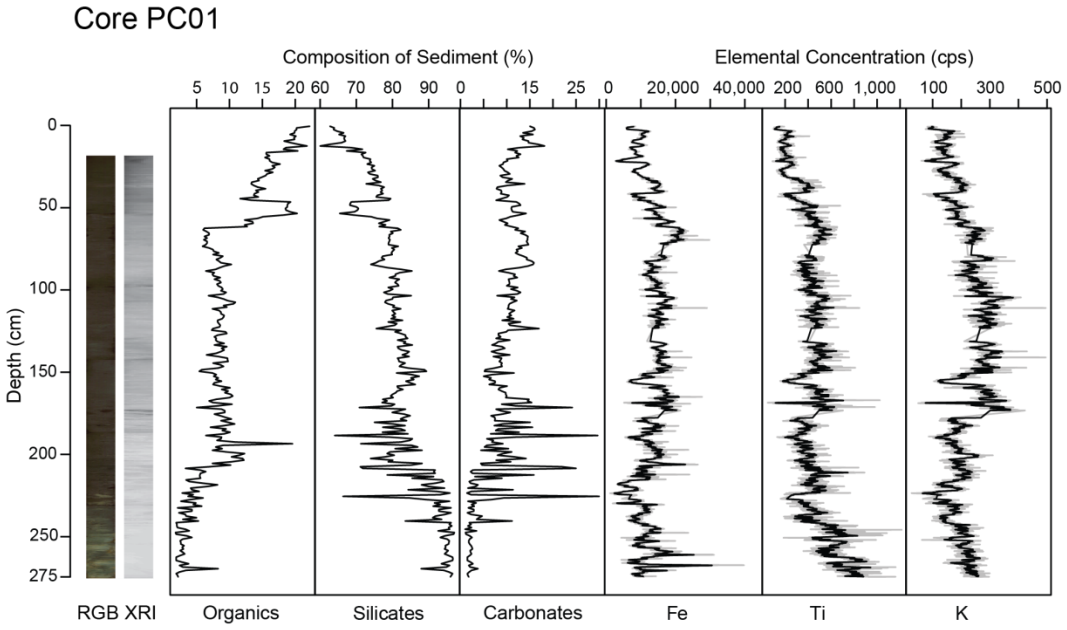

Figure 2.3: XRI and RGB images, LOI and trace element results from core PC01. From left to right: RBG and XRI images of the core; organic, silicate and carbonate content in the core represented (% of total composition), and concentration of trace elements (cps) derived from XRF values. For the XRF results, the grey line represents raw data while the black line represents the 5-point running mean.

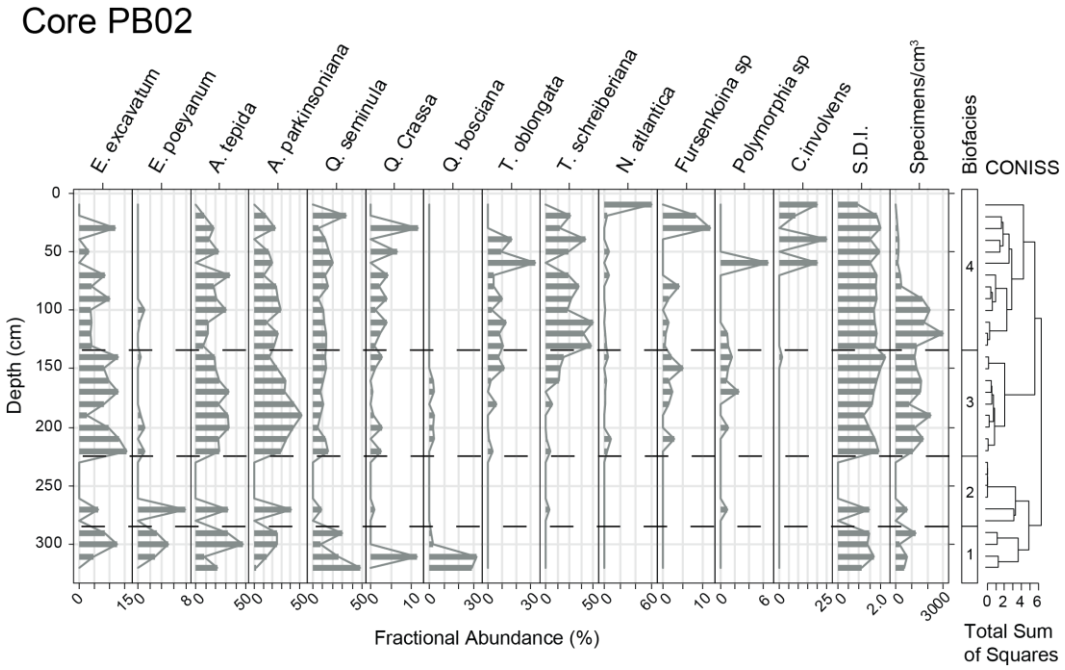

Figure 2.4: Foraminiferal results for core PB02. Foraminifera are reported as a fractional abundance. Sample diversity is represented by the Shannon-Weaver diversity index (SDI) alongside the concentration of foraminifera specimens per cm^3. The dashed black lines separate biofacies; biofacies where inferred using CONISS results plotted on the right of the figure.

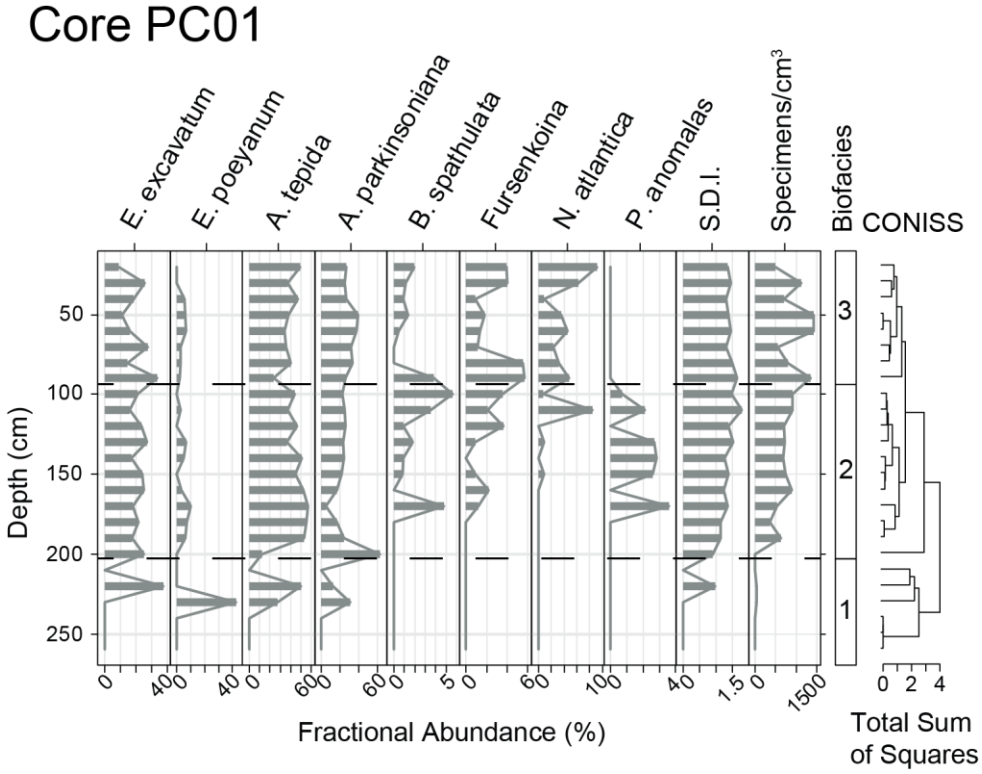

Figure 2.5: Foraminiferal results for core PC01. Foraminifera are reported as a fractional abundance. Sample diversity is represented by the Shannon-Weaver diversity index (SDI) alongside the concentration of foraminifera specimens per cm^3. The dashed black lines separate biofacies; biofacies where inferred using CONISS results plotted on the right of foraminiferal abundances.

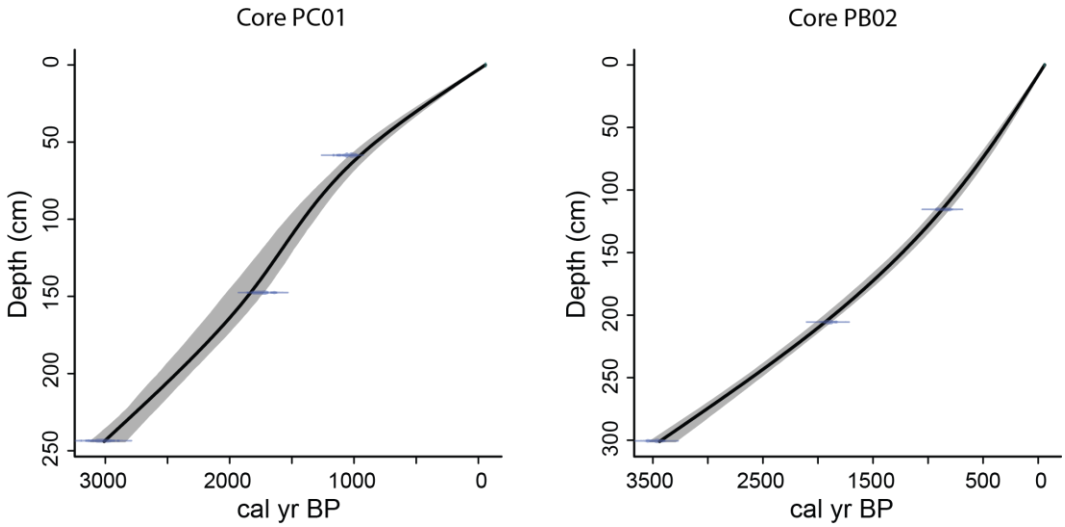

Figure 2.6: Age models for cores taken in Punta de Cartas (Left) and Playa Bailen (Right) generated using the R statistical software (CLAM package). The black line represents the "best age" calculated as a weighted average of all age-depth models generated for this core. The grey shaded regions represent 2σ confidence interval of the best age model. Dates are represented by thin blue graphs which show the calibrated age distributions for each date.

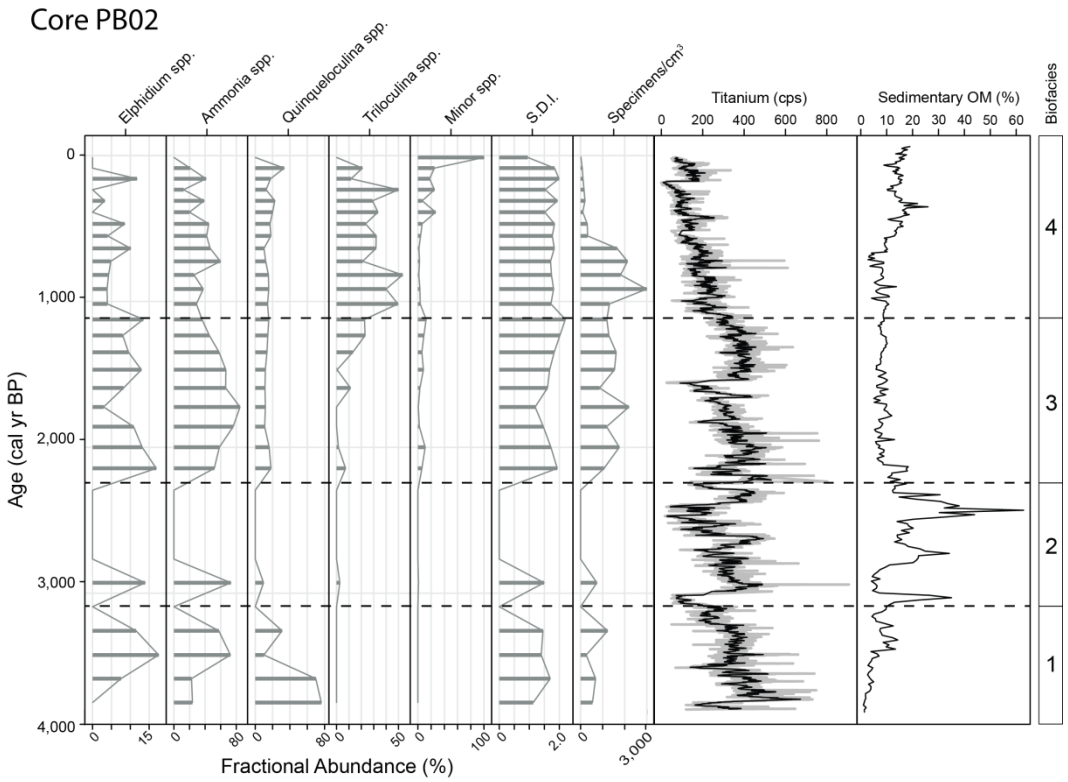

Figure 2.7: Summary of microfossil data, XRF-derived terrigenous inputs (Ti), foraminifera, OM (%) and biofacies at Playa Bailen relative to age (yr BP). Ti is used as a representation of terrigenous input as Fe and K generally follow similar trends. Biofacies are demarcated by the dashed lines

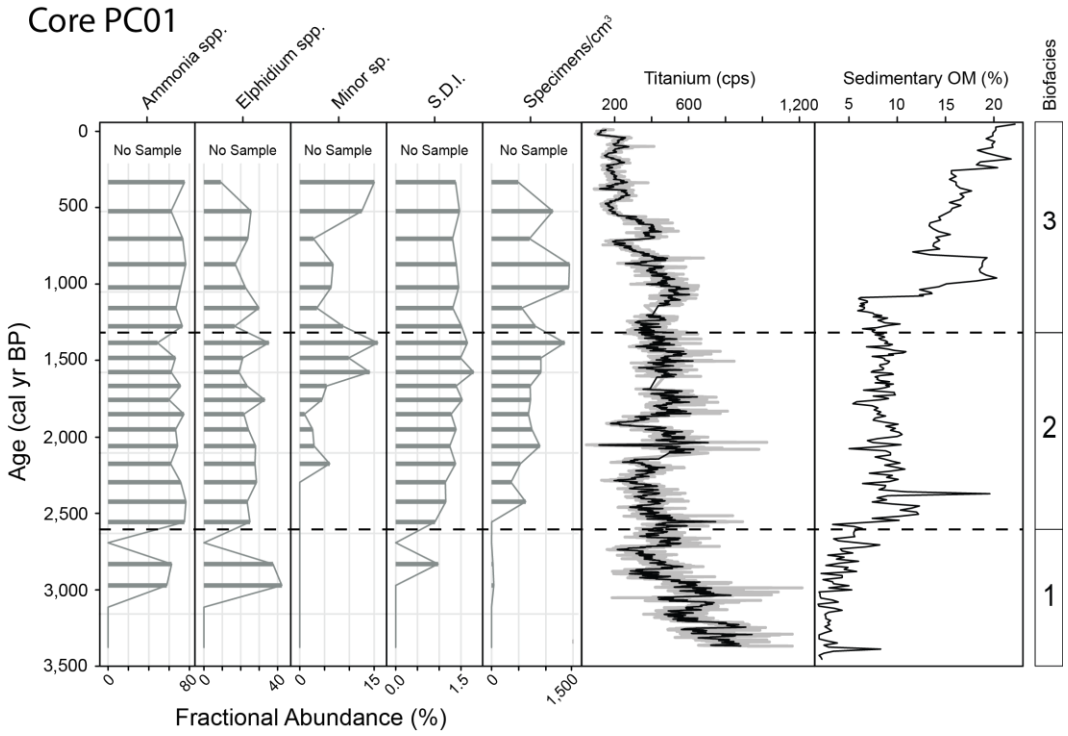

Figure 2.8: Summary diagram of microfossil data, XRF-derived terrigenous inputs (Ti), foraminifera, biofacies and OM (%) at Punta de Cartas relative to age (yr BP). Ti is used as a representation of terrigenous input as Fe and K generally follow similar trends. Biofacies are demarcated by the dashed lines

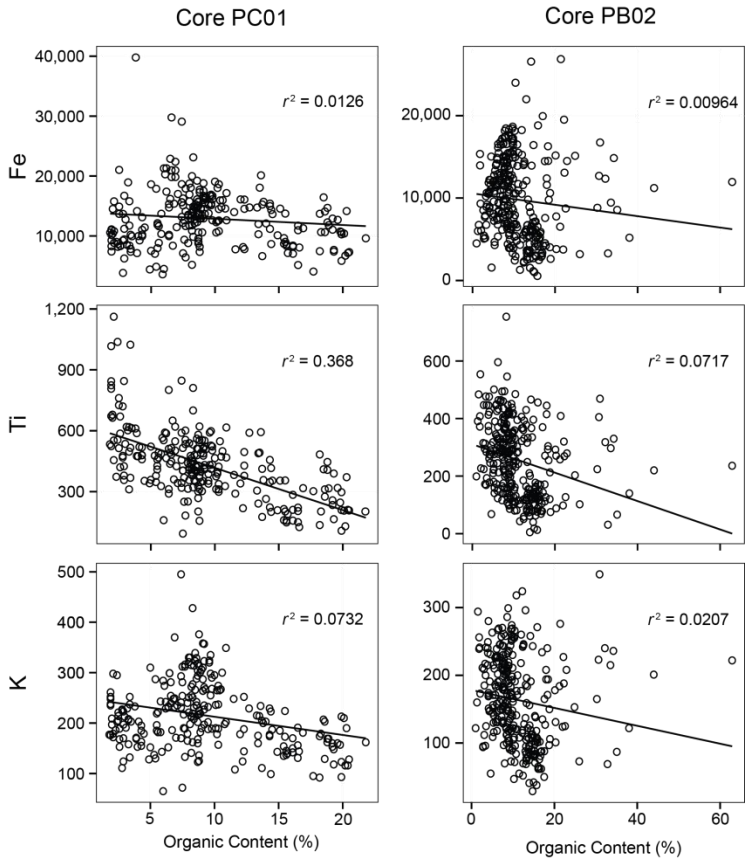

Figure 2.9: Crossplots of trace element data vs. OM in PB02 and PC01. Line of best fit is seen in each graph as the black line. Trace element values are measured in cps.

CHAPTER 2 TABLES

Table 2.1: Radiocarbon ages for Punta de Cartas (core PC01) and Playa Bailen (core PB02).

Lab ID	Sample ID	Depth (cm)	Conventional age	$\delta^{13}C$ (‰VPDB)	Calibrated yr BP (2σ)
Beta - 291719	PB02 115-116	115.5	950	-22.9	761 - 923
Beta - 291720	PB02 205-206	205.5	1950	-20	1725 - 1876
Beta - 291721	PB02 300-301	300.5	3250	-23.3	3367 - 3555
Beta - 291722	PC01 58-59	58.5	1140	-20.8	930 - 1054
Beta - 291723	PC01 147-148	147.5	1810	-21.2	1554 - 1810
Beta - 291724	PC01 243-244	243.5	2890	-22.8	2997 - 3247

CHAPTER 3

THE INFLUENCE OF MORPHOLOGY AND SEA LEVEL RISE ON SINKHOLE SEDIMENTATION: A CASE STUDY FROM LITTLE SALT SPRING, FLORIDA

Braden R.B. Gregory, Eduard G. Reinhardt, John A. Gifford

3.1 ABSTRACT

Karstic basins, because of their stable geomorphic nature, represent an ideal source of paleoclimate information in coastal systems. Despite this, relatively few studies have examined these environments from a paleoclimatogical or sedimentological perspective. In order to further develop the knowledge of the sedimentary dynamics and environmental evolution of karstic basins, a sinkhole with unique morphology on the coast of Florida was cored for paleoenvironmental analysis. Changes in grain size, loss on ignition (LOI), lithology $\delta^{13}C$, $\delta^{15}N$ and C:N results indicated four phases of deposition. Phase 1 (11 - 13.5 kyr BP) was characterized by high sediment accumulation rate, low productivity and deposition of allocthonous sediment. A decrease in accumulation marked the shift to Phase 2 (9 - 11 kyr BP) due to higher water level and uniform deposition of sediment. In Phase 3 (6.6 - 9 kyr BP), productivity increased and sedimentation was associated with autochthonous organic matter and resuspension of sediment from the upper basin of the sinkhole. During Phase 4 (0 - 6.6 kyr BP), accumulation rate decreased due to progradation of fringing wetlands on the shallow basin margin due to the deceleration of Holocene sea-level rise. Both the 'hour-glass' basin morphology and sea level rise where found to be the dominant controls on sedimentation. Though climate signals where observed during several phases, they were most obvious during periods of regular, autochthonous sedimentation.

3.2 INTRODUCTION

The coupled ocean-atmosphere systems of tropical latitudes are the main source of precipitation for North America (Schmidt et al., 2001, Wang et al., 2006, van Soelen et al., 2012). An extensive paleoclimate record for the Tropics allows for a greater understanding of how these systems can influence the climate dynamics of the nearby continents. Sediments from lacustrine systems are a common source of paleoclimate data as they preserve a wealth of proxies and act as sediment traps (Watts and Hansen, 1994, Moy et al., 2002, Donders et al., 2011, Hodell et al., 1991, Lui and Fearn, 2001, Das et al., 2013, among others). However, the archipelagos of the Caribbean do not contain an abundance of deep lakes that can be studied. Although speleothem (Fensterer et al., 2013, Mangini et al., 2007) and coastal sediments (Peros et al., 2007a,b, Donnelly and Woodruff,

2007) have been used to great effect in the past, developing additional environments for use in paleoclimate analysis will help in the development of sparse climate record of the Tropics.

Limestone is a common feature of many Caribbean islands because of the abundance of shallow, warm shelf environments conducive to high marine productivity. As these limestones age, dissolution and mechanical weathering results in the formation of karstic features (Lace and Mylroie, 2013). Karst basins, such as sinkholes, are common in coastal settings and act as sediment traps often preserving a long sedimentary record. Sinkholes contain a variety of paleoclimate proxies including pollen (Bernhardt et al., 2010), microfossils (van Hengstum et al., 2011, Gabriel et al., 2009, Kovacs et al., 2013, Alvarez-Zarikian et al., 2005) and changes in grain size (Lane et al., 2010, Brown et al., 2013). Sinkholes are therefore ideal for paleoclimate analysis in the coastal systems of the Caribbean.

Sinkholes offer advantages over other sediment sinks used in paleoclimatology. The porous nature of bedrock in karstic regions allows water table within karstic basins to track sea level (Gabriel et al., 2009, van Hengstum et al., 2011). Sinkholes deeper than 50 metres would have been inundated, and therefore recording paleoclimate information, since the early Holocene when sea level was significantly lower than present day (Brown et al., 2013, Alvarez-Zarikian et al., 2005, Shinn et al., 1996). As well, sinkholes are more stable than other coastal features whose ephemeral barrier systems can obscure paleoclimate signals. Though there are advantages of using sinkholes, particularly in tropical and subtropical areas, further understanding of the evolution of these features is needed if they are to be used as a major source of paleoclimate information.

Sinkhole sedimentation generally occurs in four stages. After the initial inundation of a sinkhole sedimentation is dominated by deposition sediment eroded from the surrounding area (Lane et al., 2011, Alvarez-Zarikian et al., 2005). As the water table rises, it is common to find highly organic peat deposits on the periphery and central breakdown pile as a marsh develops within the sinkhole (Lane et al., 2011, Gabriel et al., 2009, Kovacs et al., 2013). If there is little sediment in the surrounding area, it is possible that the marsh facies is the first deposited on bedrock (Kovacs et al., 2013, unpublished data from Casa Cenote, Mexico). As water level within the feature continues to rise, deposition of interbedded mud and coarse sediment occurs; the coarse intervals are usually associated with major runoff events washing sediment into the sinkhole from the surrounding area (Gischler et al., 2008, Brown et al., 2013, Lane et al., 2011). In an example from the Yucatan Peninsula, coarse storm deposits accounted for one third of sedimentation over the past 50 years (Brown et al., 2010). The mud deposited during this period is commonly organic (Shinn et al., 1996, Alvarez-Zarikian et al., 2005) and may be varved (Gischler et al., 2009) or laminated (Alvarez et al., 2005). Depending on the depth and location of the sinkhole

relative to the coast, this mud may be covered by marine sand containing reefal debris and show evidence of colonization by marine organisms (Kovacs et al., 2013, Shinn et al., 1996).

Though sinkholes generally follow the aforementioned sedimentary model, the morphology of the sinkhole and the surrounding region can drastically alter sinkhole sedimentation. Sinkholes with larger openings, such as the Blue Hole in Lighthouse Reef, exhibited discontinuous storm beds across several cores (Gischler et al., 2008) whereas smaller sinkholes exhibit homogenous draping sequences (Morellon et al., 2009). As well, sediment within sinkholes forms small piles under areas of concentrated sedimentation around the periphery of the sinkhole and below overhangs (Brown et al., 2013, Gischler et al., 2008). This piling of sediment can cause mass wasting events redistributing sediment throughout the sinkhole (Gischler et al., 2013, Morellon et al., 2009). Because a large portion of deposited sediments found within sinkholes is allocthonous, the development of the area surrounding sinkholes can alter the sedimentation within them. In a ~2 m core taken from a shallow sinkhole on Great Abaco Island, the Bahamas, a young peat (1.2 kyr BP) was deposited below a peat dated to ~4 kyr BP. this was interpreted to represent deposition of in situ mangrove peat overlain by allocthonous peat generated in the adjacent mangrove marsh at a much earlier date (Kovacs et al., 2013). Though water level greatly influences the sediment deposition within sinkholes (van Hengstum et al., 2011), studies suggest morphology may significantly influence the depositional regime of sinkholes. In order to further understand the influence of sinkhole morphology on sedimentation, a sinkhole near the coast of Florida with unique morphology was sampled for paleoenvironmental analysis.

3.3 STUDY AREA

3.3.1 Site Description

Little Salt Spring (LSS) is a cover-collapse sinkhole located on the west-central coast of Florida in Sarasota County approximately 20 km inland from present day Gulf of Mexico (Fig. 3.1, top). The sinkhole surface is roughly circular with a diameter of 78 m and bottom depth of 70 m below the waters` surface. Presently, water level in the feature is 5 metres above sea level (msl) placing the bottom of the sinkhole at -65 msl. The shape of the sinkhole is similar to that of an hourglass; the upper basin of the sinkhole slopes down at a 25^{o} towards a circular rim 25 - 30 m wide at -7 msl. Below this lip, the sinkhole is generally overhanging, but does not begin to widen until approximately half the distance between the rim of the upper basin and the bottom of the sinkhole (-29 msl) creating a vertical column (shaft) that connects the upper and lower basin of the sinkhole. Two prominent ledges occur in the thinner column of the sinkhole at

-21 and -13 msl. The lower basin of the sinkhole is bell-shaped expanding gradually to 60 m at its base (Alvarez-Zarikian et al., 2005, Clausen et al., 1979).

The area around LSS slopes gradually to towards SW (Fig. 3.1, bottom). To the North-East of LSS is an erosional drainage way, or slough, approximately 425 m long and 30 – 90 metres wide. This slough is the main source of overland flow into the spring. Additional hydrologic inputs into LSS include direct precipitation and lateral groundwater flow. Water is lost from the sinkhole through evaporation, groundwater seepage and surface drainage via a shallow stream to the south that connects to Big Slough, a tributary of the Myakka River, which flows into Charlotte Harbour to the southeast (Alvarez-Zarikian et al., 2005). LSS is found in a bayhead hammock with vegetation composed dominantly of *Sabal palmetto, Persea borbonea, Quercus virginiana* and *Ilex* spp. as well as several species of fern (*Archrostichum danaeaefolium, Osmunda regalis* and *O. cinnamomea*) (Brown and Cohen, 1985). Dense clusters of algae (*Chara* spp.) are found along the perimeter of the upper basin of LSS to a depth of about 3 m.

The water column of LSS shows subtle stratification near the water's surface. A chemocline exists at roughly -2 masl (7 m depth) past which water becomes anoxic and concentrations of hydrogen sulfide, nitrate and ammonium increase (Annual Project Report, NASA, 2012). Below the chemocline, the water column remains uniform with an ionic composition dominated by Na^+, Cl^- and SO_4^{2-} indicating a possible upward leakage from deep confined aquifers (Alverez-Zarikian et al., 2005).

Extremely well preserved archaeological and paleontological artifacts and shifts in ostracod assemblages to those indicative of stressed conditions suggest anaerobic conditions occurred in the upper basin of LSS since at least 7,000 yr BP (Clausen et al., 1979, Dietrich and Gifford, 1997, Alvarez-Zarikian et al., 2005). The onset of anaerobic conditions in the lower basin is uncertain and would likely have depended on autochtonous sinkhole productivity and the amount of allocthonous organic matter reaching the sinkhole.

3.3.2 Climate

Sarasota County is part of the Southern Florida Coastal Plains ecoregion characterized by humid subtropical climate (Wiken et al., 2011). The average temperature at Ft. Myers directly to the south of LSS ranges from 29 – 18^{o}C (mean 24^{o}C) with average annual precipitation of 1425 mm yearly (Florida Climate Centre, 2013). Sarasota County experiences a wet and dry season with most precipitation, up to 60%, falling between May and September. Hurricanes frequently occur during the end of the summer from August to October (Watts and Hansen, 1994).

3.3.3 Geology

The geology of the region surrounding LSS consists primarily of interbedded siliclastics and marine carbonates of Eocene to Holocene age (Wolanksy, 1983). These rocks contain three distinct aquifers: the surface aquifer system (SAS), the intermediate aquifer system (IAS) and the Floridian Aquifer system (FAS) (Wolanksy, 1983). Of primary concern to this study are the SAS and the IAS as these are the only detectable aquifers in LSS. However, upward leakage from the UFA can influence the chemical evolution of the water within LSS (Alvarez-Zarikian et al., 2005).

The SAS, the uppermost aquifer, is composed of 12 - 21 m of unconsolidated fine sands and clays of Holocene - Pliocene age (Wolansky, 1983, Hutchinson, 1992). Flow in this unit is generally to the SW and ranges from 150 - 3,000 m/day with an average value of ~400 m/day. The upper bounds of the SAS occurs ~1.5 m below the surface sediment though this varies with topography and seasonal influence (Wolansky, 1983, Duerr and Wolansky, 1986, Hutchinson, 1992).

The IAS is composed of interbedded siliclastics and permeable limestones 100 - 170 metres thick deposited from the Pliocene to mid-Miocene (Wolanksy, 1983, Sacks and Tihansky, 1996). The surface of the IAS in Sarasota county ranges from -20 to -50 msl with a potentiometric surface 3 - 10 msl (Hutchinson, 1992). Flow within this unit ranges from 150 - 275 m/day in a W to SW direction (Sacks and Tihansky, 1996, Wolansky, 1986).

3.3.4 Previous Work

There have been several studies conducted in Little Salt Spring due to its rich archaeological record. Archaeological surveys and excavations conducted at LSS in 1979 revealed artifacts on the upper basin of the sinkhole, within the sinkhole and adjacent to the sinkhole associated with the slough to the northwest. Radiocarbon dating of artifacts indicated two periods of settlement: initially from 9 - 12 kyr BP, and again from 6 - 7 kyr BP (Clausen et al., 1979). Additionally, 5 cores were taken from the centre of LSS in 1990 for the purpose of paleoclimate studies. In 2005, Alvarez-Zarikian et al. examined the paleohydrology of LSS using ostracod assemblages and oxygen isotopes from LSS Core V. Results showed gradually increasing productivity throughout the Holocene, two periods of wet, warm conditions from 5700 - 4000 yr BP and 1500 - present day, and a drier period from 2600 - 1500 yr BP coincident with a sharp increase in salinity (Alzarez-Zarikian et al., 2005).

In 2012, Bernhardt et al. presented pollen data from LSS core IV at the 13th International Palynological Congress in Tokyo, Japan (Bernhardt et al., 2010, 2012). Pollen data was divided into two major zones each containing several sub-zones (Fig. 3.2). At the base of the core, Zone Ia exhibits increased amounts of herb (Asteraceae, *Ambrosia*), grasses (Poaceae), small trees (*Morella)* and fern species. A decrease in Asteraceae in pollen zone Ib indicates more temperate conditions. The start of pollen zone Ic corresponds to the Younger Dryas (YD) which lasts until the end of pollen zone Id. The abundance of *Quercus*, *Carya* and *Morella* during this period represents drier conditions. It is also during the YD that pollen concentration begins to increase alongside the abundance of larger vascular plants (*Pinus*, *Quercus*, *Ulmus* and *Carya*). Pollen zone II is initially characterized by wetter and warmer conditions indicated by increased *Pinus* and fern pollen. Decreasing amounts of *Pinus* and ferns and increasing *Quercus* upcore indicate a drier Late Holocene. Pollen concentration increases substantially during zone II from $< 5 \times 10^5$ grains per g to $> 20 \times 10^5$ grains per g.

3.4 METHODS

In 1990, five cores where taken from the bottom of LSS (-70 msl) using submersible vibro-corer (Rossfelder) in a transect across the opening in the upper basin. Core recovery ranged from 3 - 11 m with longer cores recovered from the periphery of the sinkhole. Cores were split and stratigraphically logged. LSS Core IV which had a total length of 8.27 m was used and examined by Bernhardt et al. (2010) in the pollen study. The core was sampled at 2 cm intervals along its entire length for analysis.

Grain size was conducted at 2 cm intervals on bulk sediment samples over the entire length of the core. Bulk samples were used as sediment organic carbon (OC) and inorganic carbon (IC) was of interest for our facies analysis as they are the main sedimentary inputs to the sinkhole. Sediment samples where homogenized as a moist paste, hexameatphosphate was added, and then pre-sieved to remove > 2 mm particles, before being analyzed with a Beckman-Coulter LS 320 particle-size analyzer. Grain size distribution was converted to log scale then interpolated via a krigging algorithm and graphed in a coloured plot representing particle size distribution (PSD plot) using Geosoft Oasis software (Beierle et al., 2002, van Hengstum et al., 2006).

Loss on ignition analysis was used to quantify the amount of organic and inorganic material in samples at 10 cm intervals. Procedures followed those outlined by Heiri (2001) and Dean (1974). Approximately 1.5 cm^3 of homogenized sediment was taken from each interval and dried for 24 h at 65^{o}C. The dried sediment was then combusted at 550^{o}C for 4 h and weighed again to

determine the amount of OC in the sediment as a weight percentage (wt %). Samples were subsequently combusted again at 1000^{o}C for 2 hours in order to determine the amount of IC as wt%.

In order to examine the possibility of changing OC source, samples were analyzed for $\delta^{13}C$, $\delta^{15}N$ and the C:N ratio (Lamb et al., 2006). Sediment samples were selected at 20 cm intervals and acidified using 10% hydrochloric acid (HCl) until CO_2 release no longer occurred. After acidification, samples were rinsed and dried for 24 h at 20^{o}C then homogenized into a fine powder using a mortar and pestle. Analysis of samples took place at the McMaster Isotopologue Centre using a Delta Plus XP mass spectrometer. $\delta^{13}C$ results are expressed in permil (‰) relative to Vienna PeeDee Belemnite and $\delta^{15}N$ values in ‰ relative to diatmoic atmospheric nitrogen. The weight percentage of N (N_{Tot}) and C (C_{org}) in sample measured during isotopic analysis was converted to C:N values. The aforementioned results of geochemical and LOI analysis, as well as grain size statistics, where plotted using R statistical software with the packages ggplot2 and gridExtra (Wickham and Chang, 2012, Auguie, 2012).

Initial radiocarbon age dating of the core was conducted by Beta Analytic (Table 2). To provide a more comprehensive age-depth model for this core, additional samples of bulk organic matter and large organic matter fragments were sent to Direct AMS for radiocarbon dating. For bulk organic matter samples, larger organic fragments were selectively removed after coarsely sieving the sediment. Samples where processed using the Acid-Base-Acid pre-treatment procedures recommended by DirectAMS. Organic matter was repeatedly exposed to 6 M HCL in a 65^{o}C water bath until no evidence of reaction (discolouration, release of CO_2) occurred. Afterwards, organic matter was rinsed and exposed to a KOH solution (5g/kg) in a 65^{o}C water bath in order eliminate humic substances. When samples no longer showed signs of degradation, the base was decanted and samples rinsed with DI water. Finally, samples were rinsed with weak (0.05 M) HCL and then DI water before being dried in an oven at 60^{o}C for 24 hours and sent to Direct AMS for analysis. Raw radiocarbon ages were calibrated using the northern hemisphere terrestrial calibration curve IntCal13.14C (Reimer et al., 2013) using the R statistical software package Clam (version 2.2, Blaauw, 2010; see Table 2 for dates).The age model generated from these dates was interpolated using the smooth spline function of Clam (smooth level = 0.3); dates from depths 45, 181, 268 and 707 cm where excluded from the age model as they represent major reversals likely due to reworking or redeposition of older organic matter. An inferred date of 0 yr BP (+/- 30 yr BP) was used for the core top to represent present day.

3.5 RESULTS

3.5.1 Chronology

Nineteen dates provide temporal reference to core depth (Figure 3.3, Table 3.1). The age model generated from these ages has a 95% confidence interval ranging from 91 - 2,208 yr (mean 411 yr) and represents the last ~13,500 yr BP. Two periods of high accumulation rate occur between 575 - 817 cm (1.1 mm/yr) and from 100 - 470 cm (2.4 mm/yr) representing 11,100 - 13,500 yr BP and 6,600 - 8,200 yr BP respectively. Dates from the initial interval of higher accumulation exhibit several minor age reversals indicative of erosion and redeposition of organic matter from the upper basin of the sinkhole or reworking of sediments due to mass wasting in the lower basin of the sinkhole. The latter period of high deposition rate shows a distinct linear trend with the exception of a few larger age reversals. This suggests increased autocthonous organic matter deposition interrupted by few major redeposition events possibly related to runoff-induced erosional events or collapse of the sediment on the upper basins' rim. Sedimentation rate for the rest of the core remains much lower at 0.43 mm/yr from 470 - 575 cm (8,200 - 11,100 yr BP) and 0.15 mm/yr from 0 - 100 cm (Present day - 6,600 yr BP).

3.5.2 Lithology

3.5.2i Core description

From 529 - 827 cm (10,300 - 13,500 yr BP), sediment is dominantly composed of grey to dark-grey, quartz rich, muddy sand. Below 683 cm (11,600 yr BP), pebble sized tufa fragments and disarticulated bivalves are common implying erosion and redeposition of sediment from the upper basin of the sinkhole. Convoluted laminations are common during this period likely representing the slumping of sediment towards the central area of the basin (Gischler et al., 2008, Morellón et al., 2009). The sporadic nature of radiocarbon results during this early phase of deposition supports the reworking of sediment. Between 511 and 529 cm (9,600 - 10,300 yr BP) sediment abruptly shifts to dense clay intercalated with muddy sand. The upper 511 cm of the core (0 - 9,600 yr BP) is composed of an organic rich mud containing variable amounts of plant and finely comminuted shell fragments. Sediment is massive from 228 - 511 cm (6,900 - 9,600 yr BP) after which horizontal laminations occur until 0 cm (0 yr BP).

3.5.2ii Grain size

The mean grain size ranges from coarse sand (0.32 ϕ) to very fine silt/clay (8.21 ϕ) with an average of medium sand (1.82 ϕ; see Fig. 3.4 for details). Mode grain size values show a similar, albeit slightly finer average value of 2.04 ϕ (Fine sand) with a range between coarse sand (-0.93 ϕ) to fine silt (7.28 ϕ). Standard

deviation indicates the sediment is very poorly to poorly sorted with poorer sorting occurring during coarse intervals in the upper half of the core

At the base of the core from 529 - 827 cm (10,3000 - 13,500 yr BP), mean and mode grain size remain relatively stable at 2 ϕ. Several minor deviations of mean grain size towards finer values occur centred at 773, 713, 647 and 589 cm. The PSD plot between 529 - 827 cm shows a similar trend with a strong peak at ~3 ϕ and intervals of finer sediment concurrent with shifts observed in mean and mode grain size. Grain size distribution is generally unimodal with little spread about peak values. Finer periods are associated with bimodal distributions with a secondary peak around 6 ϕ (medium - fine silt). Shifts to finer grain size and bimodal distribution correspond to increased abundance of large vascular plants that prefer drier conditions (*Quercus*) as well as herbs and grasses (*Ambrosia*, Asteraceae, Poaceae) suggest a possible relationship between fining grain size and dry conditions. Most of these intervals fall within the Younger Dryas (11,000 - 12,000 yr BP) which several studies suggest was a relatively dry period in Florida (Bernhardt et al., 2010, Willard et al., 2007, Hughen et al., 1996).

Between 511 cm and 529 cm (9,600 - 10,300 yr BP), an abrupt shift to clay deposition occurs in the mean and mode grain size. Sorting during this interval increases to moderate and there is a strong skew towards finer values. Grain size distribution remains unimodal. This period corresponds to a brief period of distinctly increased *Quercus,* and Poaceae pollen that occurs at the termination of the YD (Bernhardt et al., 2010) suggesting a possible major drought during this interval.

After 511 cm (9,600 yr BP), mean grain size becomes more variable exhibiting alternating periods of coarse (~1.3 ϕ) and fine (~2.2 ϕ) deposition lasting until 100 cm (6,600 yr BP). Intervals of finer sediment deposition are more stable and better sorted than the coarse intervals. These variations in grain size are related to changing abundance and size of coarse organic fragments and finely comminuted shell material. PSD plot shows weaker peaks during this interval and the grain size distribution is more commonly multi-modal, with increase bi- and tri-modal distributions occurring alongside coarser grain size. Shifts to coarser values grain size correspond to periods of wetter conditions in the pollen record inferred by increased *Pinus* and fern pollen suggesting a correlation to wetter conditions at LSS.

Mean and mode values return to relatively stable values for the top 100 cm of the core (0 - 6,600 yr BP). The grain size distribution is predominantly multi-modal with a strong peak observed in the PSD plot at 0 ϕ (coarse sand) and two minor peaks at 1.5 and 3 ϕ (medium sand and very fine sand). Coarse grain size during this interval is a result of abundant organic and shell material and may be a result of buoyant organic particles settling out of suspension.

3.5.2iii Loss on Ignition Analysis

Both the OC and IC components of sediment have low values initially remaining below 5% between 11,000 and 13,500 yr BP (Fig. 3.5) indicating low productivity. Several abrupt increases in OC occur during this period with values peaking at >20% in some cases. The spikes in OC coincide with deposition of finer sediment. It is possible these shifts represent brief periods of drought resulting in reduced strength of overland flow and concentration of allocthonous organic matter deposited within the sinkhole. After 11,000 yr BP, IC increases sharply reaching a peak of 12% by ~8,000 yr BP. This may correlate to increase fine shell fragments or higher algal productivity within the sinkhole resulting in the precipitation of $CaCO_3$ (Meyers et al., 2003). The increase in IC correlates to a major shift in the $\delta^{13}C$ of from -9 ‰ to -2 ‰ in the ostracod record of LSS 11,000 yr BP observed by Alvarez-Zarikian et al. (2005). IC values decrease after 8,000 yr BP reaching 8 % at 6,500 yr BP likely caused by varying amounts of fine shell hash abundant in the sediment during this period, or the algae productivity moving away from the centre of the sinkhole due to rising water level. From 6,500 yr BP until present, IC values increase gradually reaching 11% by present day.

OC remains low longer than IC beginning to increase at ~9,000 yr BP where it more than doubles reaching ~30 % by 8,000 yr BP. OC remains between 25-40% OC until 6,500 yr BP where it increases abruptly to 60%. Values remain high until present. The increases in OC at 6,500 and 9,000 yr BP are representative of increasing productivity surrounding the sinkhole likely associated with rising water level within the feature.

3.5.3 Isotopic Geochemistry

$\delta^{13}C$ and $\delta^{15}N$ and C:N can be used to infer the source of organic matter preserved in sediments or shifts in plant communities based on the method of photosynthesis or carbon/nitrogen source used by the organism (Lamb et al., 2006, Cloern et al., 2002). Plants that use the C_3 photosynthetic pathway typically have $\delta^{13}C$ values from -21 to -32 ‰ and $\delta^{15}N$ values from -2 to 10 ‰ while plants that use the C_4 photosynthetic pathway show less discrimination against $\delta^{13}C$ resulting in isotopically lighter values between -17 and -9 ‰ (Cloern et al., 2002, Deines, 1980). Terrestrial plants have higher C:N values >12 as they are primarily composed of lignin and cellulose which are nitrogen poor (Lamb et al., 2006, Cloern et al., 2002). Aquatic plants show a wider range of values depending on whether they are using dissolved CO_2 or HCO_3^- from the water column (Lamb et al., 2006). Regardless, freshwater phytoplankton exhibits low $\delta^{13}C$ and C:N values (< -29 ‰ and 0 - 10) and higher $\delta^{15}N$ values (0 - 11 ‰) (Cloern et al., 2002).

$\delta^{13}C$ and $\delta^{15}N$ values begin relatively high at the base of the core at -24 ‰ and 7.5 ‰ respectively (Fig. 3.5). Values gradually become isotopically lighter until 8,000 yr BP. A brief interruption of this decreasing trend occurs at 10,000 yr BP where both $\delta^{13}C$ and $\delta^{15}N$ increase by ~1‰ before continuing to decrease. From 6,000 - 8,000 yr BP isotopic carbon and nitrogen become more variable and exhibit slightly enriched values. During the period from 0 - 6,600 yr BP, $\delta^{13}C$ and $\delta^{15}N$ are more stable with $\delta^{13}C$ becoming slightly enriched reaching -27.5 ‰ by present day while $\delta^{15}N$ becomes more depleted with a present day value of -1 ‰.

Carbon wt% (not shown in Fig. 3.5 due to the similarity of OC and N wt% results) and N wt % remain below 1 % from 9,200 - 13,500 yr BP. The low concentration of C and N in sediment before 9,200 yr BP may result in a bias of C:N results. Nitrogen vales in C:N represent N_{tot} values as inorganic nitrogen (N_{inorg}) is generally considered to be negligible in comparison to organic nitrogen (N_{org}). Lower organic content would therefore result in a greater influence from N_{inorg} on the C:N ratio resulting in erroneously low values. This effect is pronounced in samples with C_{org} under 1 wt% (Sampei et al., 2001). The C:N results of LSS sediment do not appear anomalously low indicating little influence from N_{inorg} in LSS sediments. However, the low values of OC in the base of the core means that even minute inclusions of allocthonous organic content my influence C:N significantly. The wt % of C and N increases after 9,000 yr BP remaining relatively high and stable until the present allowing more confidence to be placed in C:N values for this period.

C:N values at 13,500 yr BP are initially low (~15) coinciding with peaks in $\delta^{13}C$ and $\delta^{15}N$. Though these low C:N and relatively enriched isotopic C and N fall within the range of vascular C_3 plants, $\delta^{13}C$ and $\delta^{15}N$ values are higher than would generally be expected. It is possible that this deviation is related to the deposition of eroded soils from the surrounding area. An increase in soil $\delta^{13}C$ and $\delta^{15}N$ and decrease in C:N values has been observed with increasing depth in a soil profile (Nadeu et al., 2012, Lehman et al., 2002). C:N values subsequently increase after 13,000 yr BP remaining >30 until 10,500 yr BP indicating organic matter is derived predominantly from terrestrial C_3 plants.

At 10,500 yr BP, C:N decreases reaching a low of 15 by 9,000 yr BP. The lower C:N, $\delta^{13}C$ and $\delta^{15}N$ suggest an increasing amounts of freshwater algae (Cloern et al., 2002, Lamb et al., 2006). The decrease in C:N values is concurrent with larger proportion IC is sediment suggesting algal productivity played a part in controlling the IC during this period. As well, the period of lowest C:N values coincides with increasing OC suggesting that the increase in OC was due to autochthonous generation of sediment at least initially.

After the low at 10,500 yr BP, the C:N ratio continues to increase upcore reaching a value of 26 by 6,500 yr BP where it remains until present day. Gradually increasing C:N likely represents a larger portion of vascular plant debris contributing to organic matter of the sinkhole. A higher regional water table would support more vegetation on the upper basin of LSS and the surrounding area. As well, a rising water level in the sinkhole would increase the surface area of the water body exponentially as it transgressed up the basin slope increasing the area available for colonization by plants and thus the proportion of C_3 organic matter reaching the sinkholes' lower basin.

3.6 DISCUSSION

3.6.1 Water Level in LSS

Water level within karst basins is one of the main controls on sedimentation within them (van Hengstum et al., 2011). In coastal environments, water level is often approximated by sea level (Gabriel et al., 2011). However, the distance of LSS from the coast would result in a discrepancy between sea level and sinkhole water level that would closer approximate the regional water table at a given time. Presently, water level within the sinkholes is 5 masl. This may have been different during the early Holocene when variations in insolation, shifts in regional precipitation patterns and differences in evapotranspiration would influence the water level. In an attempt to simplify approximations of water level within LSS, sea level is considered the primary variable influencing water table and we assume, as is the case at present, that water level within LSS was constantly 5 masl throughout the Holocene.

3.6.2 Phase 1: Onset of deposition (11 - 13.5 kyr BP)

Sea level is an important determining factor for the inundation of LSS. However, relatively few sea level curves from the Caribbean record a signal 13,500 yr ago when sedimentation in LSS began. A minimum sea level curve generated by U-Th dating of corals off the coast of Barbados indicates sea level at this point was approximately -68 msl (Bard et al., 1990; Fig. 3.6). Similarly, reef accretion curves from Tahiti show branching *Acropora,* branching *Pocillopora* and massive *Montipora* corals (associated with water levels < 10 m below sea level) were growing at -67 msl 13,500 yr BP (Camoin et al., 2014). A recent reconstruction of Caribbean sea level by Milne and Peros (2013) that corrected peat and coral sea level points glacial isostatic adjustment, if extrapolated linearly to 13,5000 yr BP, yields a sea level of approximately -50 msl (Milne and Peros, 2013). However, sea level change during the Early Holocene was not linear (Fairbanks, 1989, Bard et al., 1990, Blanchon and Shaw 1995) biasing this estimate to shallower depths. Regardless, sea level in the Caribbean was between -50 and -68 m below its present position 13,500 yr BP indicating water in LSS

would be 2 - 15 metres deep. By the end of this phase, water level would have reached the bottom of the shaft in LSS at -29 msl.

Lithologic and geochemical results during this period suggest predominantly allocthonous deposition of material likely from the slopes of the upper basin possibly through mass wasting events (Fig. 3.7). This would have been facilitated by the sparse vegetation productivity on the upper basin inferred from low OC of the sediment. As well, the high walls of LSS would prevent sunlight from reaching the water's surface minimizing water body primary productivity (i.e. algae). Deposition was likely episodic occurring during periods of high overland flow associated with summer storms. The shallow water of the sinkhole during this phase would allow for little spread of sediment once it hit the waters' surface. Deposition would therefore be concentrated under the overhanging rim of the upper basin creating a foci of sediment deposition as observed in other sinkhole studies (Gischler et al., 2008, 2013, Brown et al., 2013). The coarser sediment would not disperse in the water body at the bottom of the sinkhole but fine sediment would, creating vertically and laterally graded sedimentation in the sinkhole. Mass wasting from the upper basin during flood events may be responsible for the convoluted laminations observed in core lithology.

As water level rose during this period, productivity would increase due to increasing incidence of sunlight on the sinkhole water body. Increasing vegetation would help in the stabilization of the upper basin. The absence of bedrock fragments after 11,700 yr BP and an increase in concentration of pollen spores after 11,500 yr BP support the conclusion of a more stable upper basin near the end of this phase.

Evidence for human settlement during this phase is sparse. A tortoise (*Geochelone crassiscutata)* shell found on a small ledge -20 msl and dated to 13,450 yr BP was surrounded by fire- hardened clay and several of its bones appeared to be carbonized (Clausen et al., 1979). The tortoise was pierced by a wooden stake dated to 12,000 yr BP. The fact that the tortoise was cooked in situ indicates water level was below - 20 msl at this point agreeing with our proposed sinkhole water level.

3.6.3 Phase 2: Sheet-like deposition (8 - 11 kyr BP)

Phase 2 corresponds to the condensed horizon observed in the age-depth model between 8,000 yr BP and 11,000 yr BP. At 11,000 yr BP, water level within LSS would have reached -28 msl (Milne and Peros, 2013) coinciding with the bottom of the sinkhole shaft. By the end of this phase, sea level rise would have pushed the water level up to rim of the upper basin at -7 msl. Several factors likely contributed to reduced accumulation rate during this phase. A large part

was the increasing deep water in LSS. A larger water column would have provided considerably more time for sediment to settle allowing for more uniform, sheet-like deposition of sediment across the sinkhole's width (Fig. 37). Piles of sediment would likely still exist during this period partially due to antecedent topography and due to reduced spread of coarser sediment resulting in a higher sedimentation below overhangs. Similar topography was observed in Chumkopo despite its larger depth of 80 m (Brown et al., 2013). Convoluted laminae remain present during this phase suggesting mass movements still occurred for some time after sinkhole initiation. Similar results were observed in Belize where mass movements were evident even in the upper metre of sediment corresponding to the last ~400 yr BP (Gischler et al., 2013). In addition to more uniform sediment deposition, ledges found along the shaft of the sinkhole would have sequestered sediment suspended at or near the water's surface. As these ledges are closer to the zone of concentrated deposition below overhangs, sediment would have a much higher chance of settling onto the ledges whereas this affect would have been minimal when water level was in the lower basin and edges further from the depositional centres. Increasing stability of the ground around LSS due to larger vegetative presence would reduce the amount of sediment reaching the sinkhole by stabilizing the upper slope and baffling sediment from the surrounding area. All these factors contributed to reduced allocthonous deposition in the area.

As this phase progresses, productivity within and around the sinkhole begins to increase. Pollen records show a larger amount of large vascular plants (Bernhardt et al., 2010). IC increases from the start of the phase marking the start of autocthonous deposition in the sinkhole. Increasing OC coincident with an inflection point of sedimentation rate at 9,000 yr BP shows the increasing importance of organic productivity to the sedimentation within LSS. By the end of this phase, autochtonous deposition of OC replaced the allocthonous deposition of the previous phase.

During Phase 2, a major period of human settlement occurs at LSS. The remnants of several informal hearths, vertebrate food refuse, wood, bone and shell artifacts, a non-returning oak boomerang, several stakes located on the edge of the sinkholes' upper basin and an oak mortar, all dating between 9,000 and 11,000 yr BP, were found at LSS (Clausen et al., 1979). LSS is thought to have served as a source of potable water for the small settlement during this period as water table was still much lower than present day (Clausen et al., 1979, Alvarez-Zarikian et al., 2005) and many Floridian lakes do not show evidence of inundation until later, around 8,000 yr BP (Watts and Hansen, 1994). Though the water level within LSS would have been much lower than present day, it would have been possible to access the water using buckets or climbing down into the sinkhole. Several stakes found around the periphery of LSS dated between 9,500 and 10,500 yr BP are thought to be used for this purpose (Gifford, *personal*

communication). At 10,000 yr BP, water level within the feature would have been at -20 msl coinciding with a large ledge on which the remains of a cooked tortoise were found. Additional faunal remnants are scattered along this shelf including small freshwater turtles, rattlesnakes, rabbits and an immature mastodon (Clausen et al., 1979). The predominance of faunal remains are likely the result of animals falling into the sinkhole and swimming to this shelf in an attempt to escape only to starve to death when they could not climb past the overhang rim of the upper basin above them. The sinkhole acting as a natural trap for game would further encourage humans to settle LSS. The settlement is thought to have been abandoned at approximately 9,000 yr BP around the time when this ledge would have been flooded. Previous authors associated the abandonment of LSS with widespread wet conditions throughout Florida and higher water table thus reducing the need to use LSS as a water source (Clausen et al., 1979, Alvarez-Zarikian et al., 2005). Though pollen data from our core and the nearby slough corroborate this conclusion (Clausen et al., 1979, Bernhardt et al., 2010), the drowning of the shelf may have served as further encouragement to abandon LSS

3.6.4 Phase 3: High Upper Basin Productivity (6.6 - 8 kyr BP)

Phase 3 represents a period of high, stable sedimentation lasting from 6,600 - 8,000 yr BP. Water level during this period would have increased from the rim of the sinkhole at - 7 msl into the upper basin reaching -5 msl by 6,600 yr BP. As water level transgressed up the upper basin of LSS, sediment transport into the sinkhole would have changed. Increasing OC and a stronger signal from C_3 plants during this period indicates the presence of fringing vegetation around the periphery of LSS. This vegetation would baffle sediment brought into the lagoon by overland flow reducing the amount of allocthonous sediment input into LSS. Sediment transport from the upper to lower basin would occur through gravitation movement of sediment down-slope via micro- and macro-mass wasting as well as through the resuspension of sediment from the slopes of the upper basin during periods of lower wave base (e.g. summer storms) (Fig. 3.7). Buoyant organic matter and slow settling sediment may also find its way to the centre of LSS and slowly fall out of suspension over time.

Several large age reversals (~500 - 1500 yr BP) occur during this period representing redeposition of old organic matter though none of the age reversals provides an age earlier than the initiation of this phase (8,000 yr BP). These periods may correspond to major runoff events. However, grain size does not appear to coarsen during these periods as is generally observed in sinkhole storm deposits (Gischler et al., 2013, Brown et al., 2013, Lane et al., 2010). Instead, these events may represent a failure of the slope at the lip of the sinkhole resulting in the redeposition of organic matter deposited during colonization of the upper basin rim when water level was lower.

The minor changes in grain size during this period are associated with variations in fine shell content and organic fragments may be representative of changes in local climate. Periods with finer grain size and better sorting correlate to higher abundances population of "wet" plant species such as pines and ferns while coarser intervals correlate to decreased abundance of these species (Bernhardt et al., 2010). The finer periods also roughly correlate to increased incidence of El Niño/the Southern Oscillation (ENSO) events observed in Southern Ecuador (Moy et al., 2002) and warmer sea surface temperatures in the Orca Basin of the Gulf of Mexico (LoDico et al., 2006). ENSO has been correlated to increased precipitation, an elevated regional water table and higher rate of stream flow in Florida (Beckage et al., 2003, Sun and Furbish, 1997, Donders et al., 2005) as well, as a decrease in Atlantic hurricane activity (Gray 1984, Donnelly and Woodruff, 2007). Similarly, warm SST in the Gulf of Mexico correlate with increased precipitation in Peninsular Florida (Donders et al., 2009, Wang et al., 2006). We posit that the higher precipitation values caused by warmer temperatures in the Gulf of Mexico and stronger ENSO as well as decreased storm activity around Florida would result in higher water levels within the LSS and decreased resuspension of coarse organic matter in the upper basin resulting in finer, mores stable deposition. Conversely, increased storm activity and slightly lower water level would result in chaotic unstable deposition of coarse, possibly allocthonous material. This would result in an overall shift to finer, better-sorted sediment. Unfortunately, there are few storm records for the Caribbean that reach the mid to early Holocene for comparison in order to further test this hypothesis.

3.6.5 Phase 4: System Equilibrium (0 - 6.6 kyr BP)

Starting at 6,600 yr BP, accumulation of sediment at LSS drops sharply to the lowest observed values in the core. Several Caribbean sea level reconstructions show a hinge point occurring between 6 and 7 kyr BP in which the rate of sea level rise decreases dramatically (Toscano and Macintyre, 2003, Gischler and Hudson, 2004, Milne and Peros, 2013, Camoin et al., 2014, among others). The water level rise in LSS would also decelerate. Water level within the feature would have only increased from -5 masl to 5 masl over the past 6,600 yr BP. The deceleration of water level coupled with the shallow sloping sides of the upper basin would allow vegetation productivity on the periphery to keep pace or even surpass rising water level resulting in progradation of vegetation. Increased baffling and sequestration of sediment on the periphery of the upper basin would occur restricting transport of allocthonous material into the sinkhole. As well, a larger surface area on the upper basin produced by higher water level would increase the deposition of sediment on the upper slopes of the basin reducing the amount of sediment reaching the centre of the sinkhole via mass movement (Fig. 3.7). Most deposition into the sinkhole during this phase would likely come from buoyant organic and shell material floating out to the centre of the sinkhole and

gradually falling out of suspension. The laminations that reappear during this phase are may be representative of stronger seasonality and anoxic bottom water conditions where alternations between strong summer storms depositing coarse organic matter from the upper basin and calm dry seasons depositing silt and clay from suspension settling would occur.

The initiation of this final phase correlates with the Archaic settlement at LSS. A major settlement near the slough to the northeast of LSS is present from roughly 5,200 - 6,800 yr BP evidenced by an extensive graveyard containing >1000 individuals and abundant human artifacts and vertebrate refuse covering 10,000 - 20,000 m^2. Decreased regional water table associated with drier conditions during this period is the cause of LSS settlement, as it may have acted as a source of potable water. Pollen evidence from LSS, however, does not suggest conditions were drier than previously observed (Bernhardt et al., 2010). Similarly, pollen records from Lake Tulane and Sheelar Lake in central Florida do not indicate conditions any drier than earlier in the Holocene (Watts and Hansen, 1994, Grimm et al., 2006). Perhaps the increase in water body size from large pond to small lake or the availability of peat in which the Archaic people preferred to inter their bodies that encouraged the resettlement of LSS. Pollen data from around Florida does suggest increased wetness after 5000 yr BP broadly agreeing with the conclusion of site abandonment due to widespread water availability during this period (Watts and Hansen, 1994).

3.7 CONCLUSION

Analysis of core lithology and isotopic geochemistry of LSS core IV indicated four main phases of deposition. Phase 1 (11 - 13.5 kyr BP) was characterized by allocthonous sediment deposition from the surrounding area, high accumulation and low productivity. During phase 2 (9 - 11 kyr BP) a larger water column and more stable upper slope significantly reduced the accumulation rate of sediment and resulted in uniform, sheet-like deposition. As productivity increased, the sinkhole shifted to Phase 3 (6.6 - 9 kyr BP) represented by deposition autocthonous, organic rich sediment. After 6,600 yr BP the sinkhole reached an equilibrium with the surrounding area resulting in sediment starvation. Previous studies suggested water level as the dominant control on sedimentary dynamics in sinkholes. However, the evolution of deposition in LSS was controlled by the water level within the sinkhole and how it interacted with the sinkhole's morphology.

Though there was no clear correlation to climate during the LSS record, several shifts in grain size and OC did correlate to climate related shifts in pollen content of the core. During phase 1, brief periods of finer grain size and increased OC correlated to increased *Quercus,* grasses and shrubs (Bernhardt et al., 2010) suggesting drier periods. However, there is no evidence of wetter periods being

recorded during this phase. Poor age control due to episodic deposition and frequent reworking of sediment during this period may have altered the sedimentary record reducing the confidence in the timing of these events. During Phase 3, periods of increasing and decreasing grain size associated with changing organic content correlate well with regional controls on climate suggesting climate played a role in these shifts. The more apparent response to climate during phase 3 suggests that periods of stable accumulation are best suited for examining paleoclimate emphasizing the need for extensive dating when attempting to reconstruction paleoenvironment from sinkhole sediment.

REFERENCES

Alvarez-Zarikian, C.A., Swart, P.K., Gifford, J.A. and Blackwelder, P.L. (2005). Holocene paleohydrology of Little Salt Spring, Florida, based on ostracod assemblages and stable isotopes. *Palaeo3,* 225, 134-156.

Auguie, B. (2012). gridExtra: functions in grid graphics. Retrieved from http://cran.R-project.org/package=gridExtra.

Bard E., Hamelin, B., Fairbanks, R.G. and Zindler, A. (1990). Calibration of the ^{14}C timescale over the past 30,000 years using mass spectrometric U-Th ages from Barbados corals. *Nature,* 345, 405-410.

Beckage, B., Platt, W.J., Slocum, M.G. and Panko, B. (2003). Influence of the El Niño Southern Oscillation on the fire regimes in the Florida everglades. *Ecology*, 84, 3124-3130.

Bernhardt, C.E., Willard, D., Landacre, B. and Gifford, J. (2010). Vegetation changes during the last deglacial and early Holocene: a record from Little Salt Spring, Florida (Abstract #PP41B-1635). *Proceedings from AGU ’10: The American Geophysical Union Fall Meeting,* San Francisco, CA.

Bernhardt, C.E., Willard, D.A. and Gifford, J. (2012). Pollen evidence for a cool, dry Younger Dryas and warm, wet Early Holocene in the southeastern United States, Abstract. *Proceedings from the IPC ’12: the 13th International Palynological Congress*, Tokyo, Japan.

Beierle, B.D., Lamoureux, S.F., Cockburn, J.M.H. and Spooner, I. (2002). A new method for visualizing sediment particle size distributions. *Journal of Paleolimnlogy,* 27, 279-283.

Blaauw, M. (2010). Methods and code for “classical” age-modelling of radiocarbon sequences. *Quaternary Geochronology,* 5, 512-518.

Blanchon, P. and Shaw, J. (1995). Reef drowning during the last deglaciation:Evidence for catastrophic sea-level rise and ice-sheet collapse. *Geology,* 23, 4-8.

Brown, A., Reinhardt, E.G., van Hengstum, P.J. and Pilarcyzk, J.E. (2013). A coastal Yucatan sinkhole records intense hurricane events. *Journal of Coastal Research,* 294, 418-428.

Camoin, G.F., Seard, C., Deschamps, P., Webster, J.M, Abbey, E., Braga., J.C., Iryu, Y., Durand, N., Bard, E., Hamelin, B., Yokoyama, Y., Thomas, A.L.,

Henderson, G.M. and Dussoiullez, P. (2012). Reef response to sea-level and environmental changes during the last deglaciation: Integrated Ocean Drilling Program Expedition 310, Tahiti Sea Level. *Geology*, 40, 643-646

Clausen, C.J., Cohen, A.D., Emiliani, C. Holman, J.A. and Stipp , J.J. (1979). Little Salt Spring Florida: A unique underwater site. *Science,* 203, 609-614.

Cloern, J.E., Canuel, E.A. and Harris, D. (2002). Stable Carbon and Nitrogen isotope composition of aquatic and terrestrial plants of the San Francisco Bay estaurine system. *Limnology and oceanography*, 47, 713-729.

Dean, W.E. (1974). Determination of carbonate and organic matter in calcareous sediments and sedimentary rocks by loss on ignition: comparison with other methods. *Journal of Sedimentary Petrology,* 44, 242-248.

Deines, P. (1980). The isotopic composition of reduced organic carbon. In: Fritz, P. and Fontes, J.C. *Handbook of Environmental Geochemistry, vol. 1: the Terrestrial Environment* (329-406). Amersterdam: Elsevier.

Dietrich, P.M. and Gifford, J.A. (1997). Depositional sequence at Little Salt Spring (8So18): Paleoenvironmental implications for Pleistocene-Holocene noundary in Peninsular Florida. Abstract, *Geological Society of America Bulletin,* Southeastern Section Meeting.

Donders, T.H., Wagner, F., Dilcher, D.L. and Visscher, H. (2005). Mid- to late-Holocene El Niño-Southern Oscillation dynamics reflected in the subtropical terrestrial realm. *Proceedings of the National Academy of Sciences of the United States of America,* 102, 10904-10908.

Donders, T.H., de Boer, H.J., Finsinger, W. Grimm, E.C., Dekker, S.C., Reichart, G.J. and Wagner-Cremer, F. (2009). Impact of the Atlantic Warm Pool on precipitation and temperature in Florida during North Atlantic cold spells. *Climate Dynamics,* 36, 109-118.

Donnelly, J.P. and Woodruff, J.D. (2007). Intense hurricane activity over the past 5000 years controlled by El Nino and the West African monsoon. *Nature,* 447, 465-468.

Fairbanks, R.G. (1989). A 17,000-year glacio-eustatic sea level record: influence of glacial melting rates on the Younger Dryas event and deep-ocean circulation. *Nature,* 342, 637-641.

Fensterer, C., Scholz, D., Hoffman, D.L., Spötl, C., Schröder-Ritzrau, A., Horn, C., Pajón, J.M and Mangini, A. (2013). *Earth and Planetary Science Letters,* 361, 143-151.

Florida Climate Centre. (2013). Ft Myers precipitation and temperature trends, monthly values from 1900 - 2010 [table]. Retrieved from http://climatecenter.fsu.edu/products-services/data

Gabriel, J.J., Reinhardt, E.G., Peros, M.C., Davidson, D.E., van Hengstum, P.J. and Beddows, P.A. (2008). Palaeoenvironmental evolution of Cenote Aktun Ha (Carwash) on the Yucatan Peninsula, Mexico, and its response to Holocene sea-level rise. *Journal of Paleolimnology*, 42, 199-213.

Gischler, E. and Hudson, J. (2004). Holocene development of the Belize Barrier Reef. *Sedimentary Geology,* 164, 223-236.

Gischler, E., Shinn, E.A., Oschmann, W., Fiebig, J. and Buster, N.A. (2008). A 1500-year Holocene Caribbean climate archive from the Blue Hole, Lighthouse Reef, Belize. *Journal of Coastal Research,* 246, 1495-1505.

Gischler, E., Anserlmetti, F.S. and Shinn, E.A. (2013). Seismic stratigraphy of Blue Hole (Lighthouse Reef, Belize), a late Holocene climate and storm archive. *Marine Geology,* 344, 155-162.

Gray, W.M. (1984). Atlantic seasonal hurricane frequency. Part 1: El Niño and 30 mb quasi-biennial oscillation influences. *Monthly Weather Review,* 112, 1649-1668.

Grimm, E.C., Jacobson, G.L., Watts Jr., W.A., Hansen, B.C.S and Maasch, K.A. (1993). A 50,000-year record of climate oscillations from Florida and its temporal correlation with Heinrich Events. *Science,* 261, 198-200.

Heiri, O., Lotter, A.F. and Lemcke, G. (2001). Loss on ignition as a method for estimating organic and carbonate content in sediments: reproducibility and comparability of results. *Journal of Paleolimnology,* 25, 101-110.

Hodell, D.A., Curtis, J.H., Jones, G.A., Higuera-Gundy, A., Brenner, M., Binford, M.W., and Dorsey, K.T. (1991). Reconstruction of Caribbean climate change over the past 10,500 years. *Letters to Nature,* 352, 790 - 793.

Hughen, K.A., Overpeck, J.T., Peterson, L.C. and Trumbore, S. (1996). Rapid climate changes in the tropical Atlantic region during the last deglaciation. *Nature,* 380, 51-54.

Hutchinson, C.B. (1992). Assessment of hydrogeologic conditions with emphasis on water quality and wastewater injection, southwest Sarasota and West Charlotte Counties, Florida. *U.S. Geological Survey,* Water Supply Paper 2371.

Kovacs, S.E., van Hengstum, P.J., Reinhardt, E.G., Donnelly, J.P. Albury, N.A. (2013). Late Holocene sedimentation and hydrologic development in a shallow coastal sinkhole on Great Abaco Island, The Bahamas. *Quaternary International,* 317, 118-132.

Lamb, A.L., Wilson, G.P. and Leng, M.J. (2006). A review of coastal palaeoclimate and relative sea-level constructions using ^{13}C and C/N ratios in organic material. *Earth-Science Reviews,* 75, 29-57.

Lane, P., Donnelly, J. Woodruff, J.D. and Hawkes, A.D. (2011). A decadelly-resolved paleohurricane record archived in the late Holocene sediments of a Florida sinkhole. *Marine Geology,* 287, 14-30.

Liu, K. and Fern, M.L. (2000). Reconstruction of prehistoric landfall frequencies of catastrophic hurricanes in northwestern Florida from lake sediment records. *Quaternary Research,* 54, 238-245.

LoDico, J.M., Flower, B.P and Quinn, T.M. (2006). Subcentennial-scale climatic and hydrologic variability in the Gulf of Mexico during the early Holocene. *Paleoceanography,* 21, PA3015.

Mangini, A., Blumbach, P., Verdes, P, Spötl, C., SCholz, D., Machel, H. and Mahon, S. (2007). *Quaternary Science Reviews,* 26, 1332-1343.

Meyers, P.A. (2003). Applications of organic geochemistry to paleolimnological reconstructions: a summary of examples from the Laurentian Great Lakes. *Organic geochemistry,* 34, 261-289.

Milne, G.A. and Peros, M. (2013). Data-model comparison of Holocene sea-level change in the circum-Caribbean region. *Global and Planetary Change,* 107, 119-131.

Morellón, M., Valero-Garcés, B., Anselmetti, F., Ariztegui, D., SChnellmann, M., Moreno, A., Mata, P., Rico, M. and Corella, J.P. (2009). Late Quaternary deposition and facies model for karstic lake Estanya (Noerth-eastern Spain). *Sedimentology,* 56, 1505-1534.

Moy, C.M. Seltzer, G.O., Rodbell, D.T. and Anderson, D.M. (2002). Variability of El Niño/Southern Oscillation activity at millennial timescales during the Holocene epoch. *Nature,* 420, 162 - 165.

Mylroie, J.E. (2013). Coastal Karst Development in Carbonate Rocks. In Lace , M. and Mylorie, J. *Coastal Karst Landforms* (77 - 109). Boca Raton, Fl: Springer.

Nadeu, E., Berhe, A.A., de Vente, J. and Boix-Fayos, C. (2012). Erosion, deposition and replacement of soil organic carbon in Mediterranean catchments: a geomorphological, isotopic and land use change approach. *Biogeosciences,* 9, 1099-1111.

NASA. (2012). Biosignatures in relevant microbial ecosystems: 2012 Annual report from the Penn State Astrobiology Research Centre. Retrieved from http://astrobiology.nasa.gov/nai/reports/annual-reports/2012/psu/biosignatures-in-relevant-microbial-ecosystems/

Peros, M.C., Reinhardt, E.G., Schwarez, H.P. and Davis, A.M. (2007). High-resolution paleosalinity reconstruction from Laguna de la Leche, north coastal Cuba, using Sr, O, and C isotopes. *Paleo3,* 245, 535-550

Peros, M.C., Reinhardt, E.G. and Davis, A.M. (2007). A 6000-year record of ecological and hydrological changes from Laguna de la Leche, north coastal Cuba. *Quaternary Research,* 67, 69-82.

Reimer, P.J., Bard, E., Bayliss, A., Beck, J.W., Blackwell, P.G., Bronk Rmasey, C., Buck, C.E., Edwards, R.L., Friedrich, M., Grootes, P.M., Guilderson, T.P., Haflidason, H., Hajdas, I., Hatté, C., Heaton, T.J., Hoffman, D.L.,

Hogg, A.G., Hughen, K.A., Kaiser, K.F., Kromer, B., Manning, S.W., Niu, M., Reimer, R.W., Richards, D.A., Scott, DE.M., Southon, J.R., Turney, C.S.M. and van der Plicht, J. (2013). IntCal13 and Marine13 radiocarbon age calibration curves, 0-50,000 years cal BP. *Radiocarbon,* 55, 1869-1887

Sacks, L.A. and Tihansky, A.B. (1996). Geochemical and isotopic composition of ground water, with emphasis on sources of sulfate in the Upper Floridan Aquifer and Intermediate Aquifer System in southwest Florida. *U.S. Geological survey,* Water-Resources Investigations Report 96-4146.

Sampei, Y. and Matsumoto, E. (2001). C/N ratios in a sediment core from Nakaumi Lagoon, southwest Japan - usefulness as an organic source indicator. *Geochemical Journal,* 35, 189-205.

Schmidt, N., Lipp, E.K., Rose, J.B. and Luther, M.E. (2001). ENSO influences on seasonal rainfall and river discharge in Florida. *Journal of Climate,* 15, 615-627.

Shinn, E.A., Reich, C.D., Locker, S.D. and Hine, A.C. (1996). A giant sedimentary trap in the Florida Keys. *Journal of Coastal Research,* 12, 953-959.

Sun, H. and Furbish, D.J. (1997). Annual precipitation and river discharges in Florida in response to El Niño - and La Niña-sea surface temperature anomalies. *Journal of Hydrology,* 199, 74-87.

van Hengstum, P.J., Reinhardt, E.G., Boyce, J.I. and Clark, C. (2006). Changing sedimentation patterns due to historical land-use change in Frenchman's Bay, Pickering, Canada: evidence from high-resolution textural analysis. *Journal of Paleolimnology,* 37, 603-618.

van Hengstum, P.J., Scott, D.B., Gröcke, D.R. and Charette, M.A. (2011). Sea level controls sedimentation and environments in coastal caves and sinkholes. *Marine Geology,* 286, 35-50.

van Soelen, E.E., Brooks, G.R., Larson, R.A., Sinnighe-Damsté, J.S. and Reichart, G.J. (2012)/ Mid- to Late- Holocene coastal environmental changes in southwest Florida, USA. *The Holocene,* 22, 929-938.

Wang, C., Enfield, D.B., Lee, S.-K. and Landsea, C.W. (2006). Influences of the Atlantic warm pool on Western Hemisphere summer rainfall and Atlantic hurricanes. *Journal of Climate,* 19, 3011-3028.

Watts. W.A. and Hansen, B.C.S. (1994). Pre-Holocene and Holocene pollen records of vegetation history from the Florida peninsula and their climatic implications. *Paleo3,* 109, 163-176.

Wickham, H. (2009). Ggplot2: elegant graphics for data analysis. *Springer New York.*

Wiken, E., Francisco, J.N. and Griffith, G. (2011). North American Terrestrial Ecoregions - Level III. *Commission for Environmental Cooperation,* Montreal, Canada.

Willard, D.A., Bernhardt, C.E., Brooks, G.R., Cronin, T.M., Edgar, T. and Larson, R. (2007). Deglacial climate variability in central Florida, USA. *Palaeo3,* 251, 366-382.

Wolansky, R.M. (1983). Hydrogeology of the Sarasota-Port Charlotte area, Florida. *U.S. Geological Survey,* Water-Resources Investigations Report 82-4089.

CHAPTER 3 FIGURES

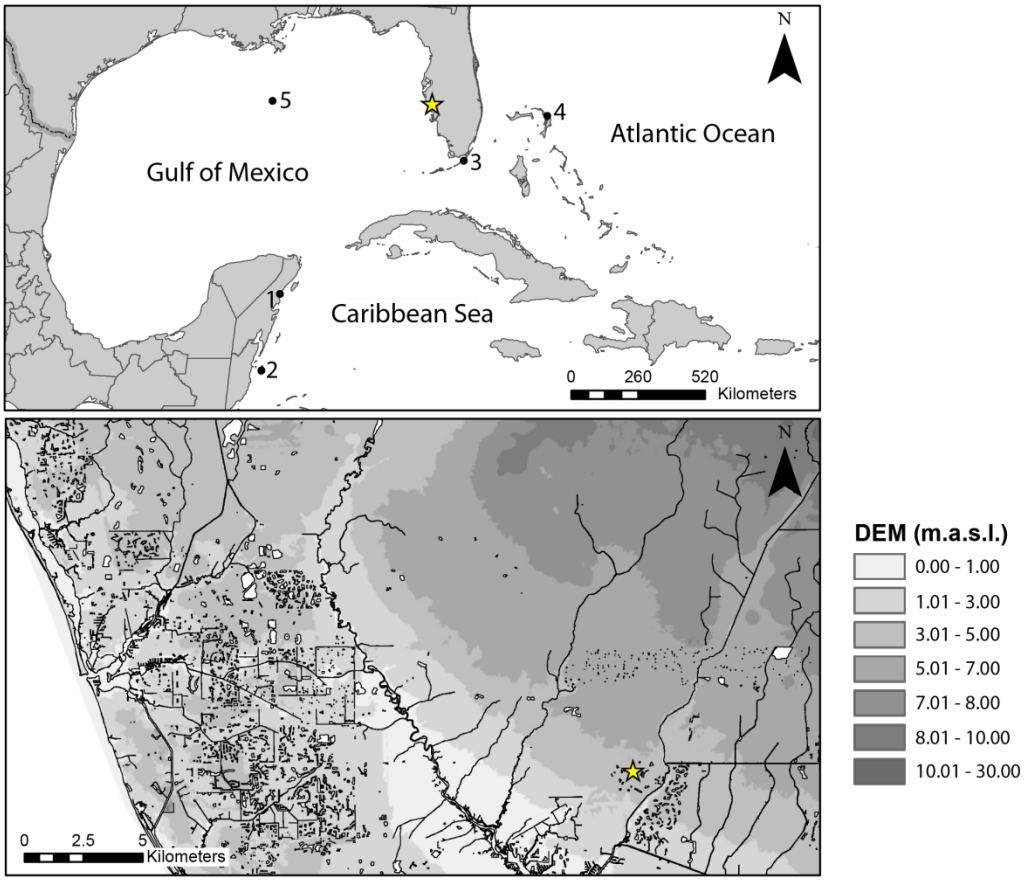

Figure 3.1: (top) Location of LSS in the context of the greater Caribbean; other study sites mentioned in this paper are shown as number black dots. LSS is denoted by the yellow star. Other locations include (1) Chumkopo, Yucatan Peninsula (Brown et al., 2013); (2) Lighthouse Reef, Belize (Gishler et al., 2008, 2013); (3) Unnamed Florida sinkhole, Florida (Shinn et al., 1996); (4) Great Abaco Island, the Bahamas (Kovacs et al., 2013); (5) Orca Basin, Gulf of Mexico (LoDico et al., 2006). (Bottom) DEM of Sarasota County and position of LSS relative to the Gulf of Mexico. Water bodies and rivers are white outlined in black.

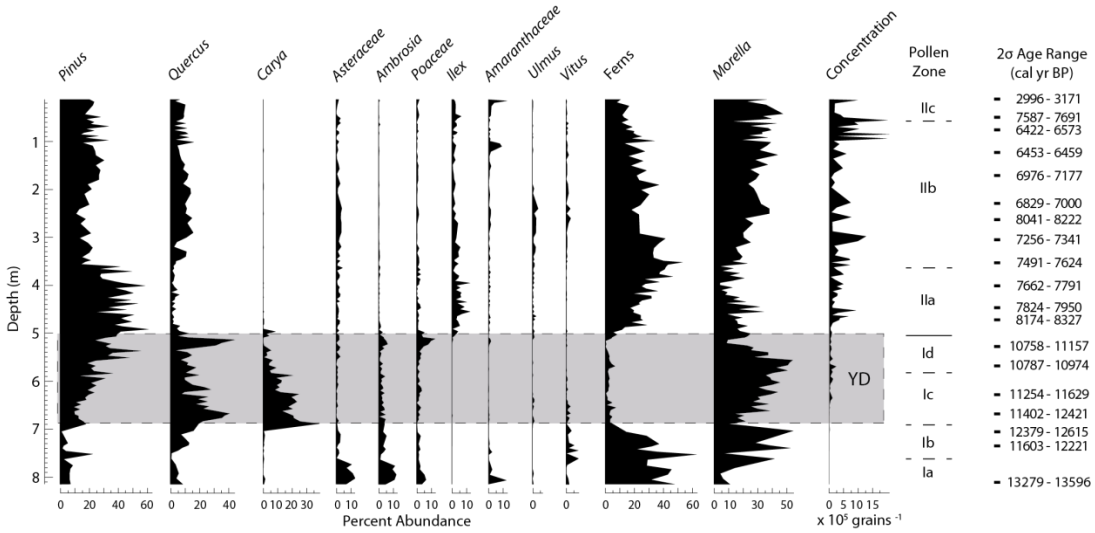

Figure 3.2: Pollen diagram for LSS core IV reproduced from Bernhardt et al. (2010) and 2σ age range of dates generated in this study. The gray bar represents the Younger Dryas (YD).

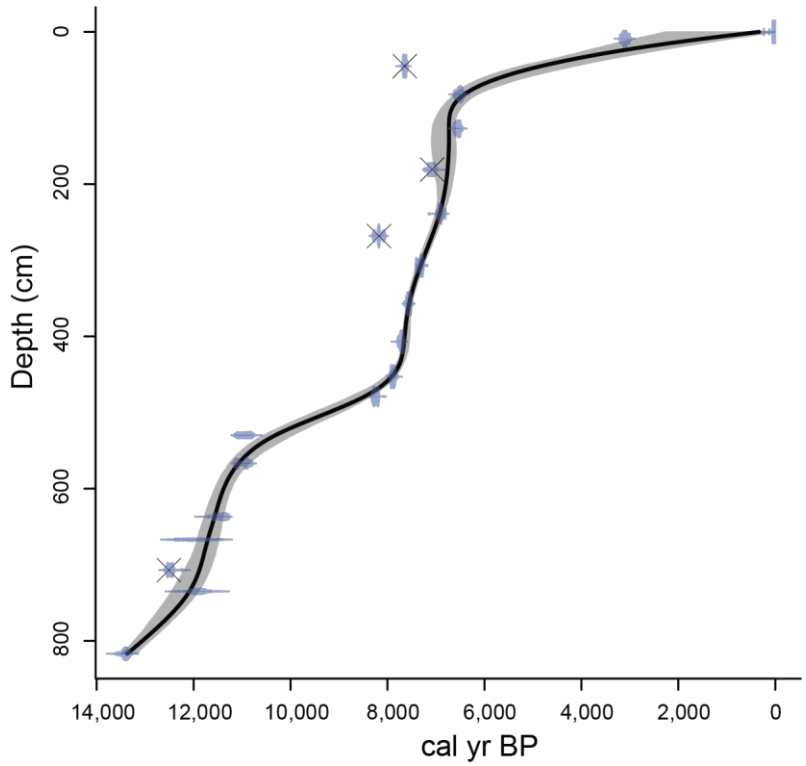

Figure 3.3: Age-depth model for LSS sediments generated with the Clam package for R statistical software. The black line represents the age-weighted mean value for a given depth. The grey shaded area corresponds to the 95% confidence interval for the age-depth model. Dated intervals are represented by the miniature blue graphs, which show the calibrated distribution of ages for a given date. Dates with a black "X" through them were removed before generation of the age model to minimize age reversals.

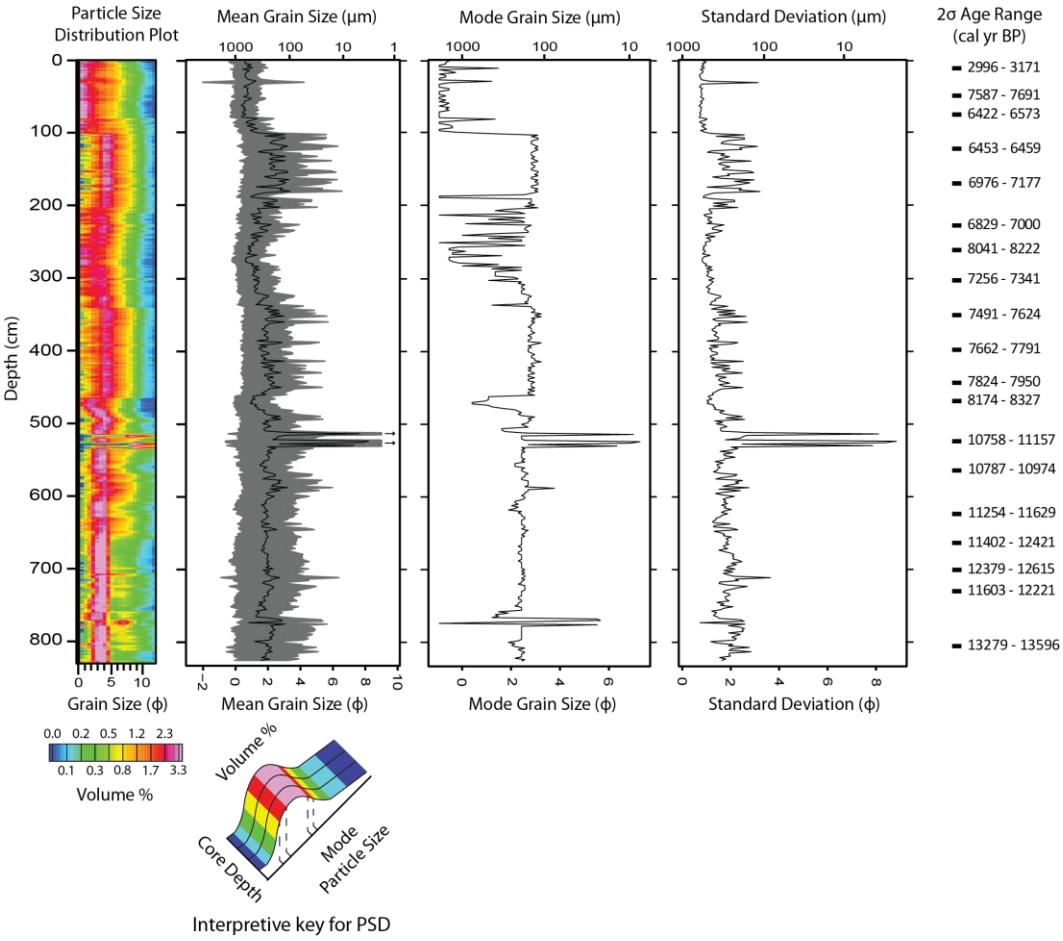

Figure 3.4: Grain size sample statistics (mean, mode, standard deviation) alongside interpolated particle size distribution (PSD) plot for LSS core IV. The grey ribbon on mean grain size represents the within-sample standard deviation and the black line represents sample mean value. The x-axis of the PSD represent grain size (ϕ), the y-axis represents depth in core and the z-axis, represented with color, indicates % volume of sediment. Warmer colours (pink, red) indicate higher volume % of sediment. See identification key for a visual description of how to interpret PSD plots.

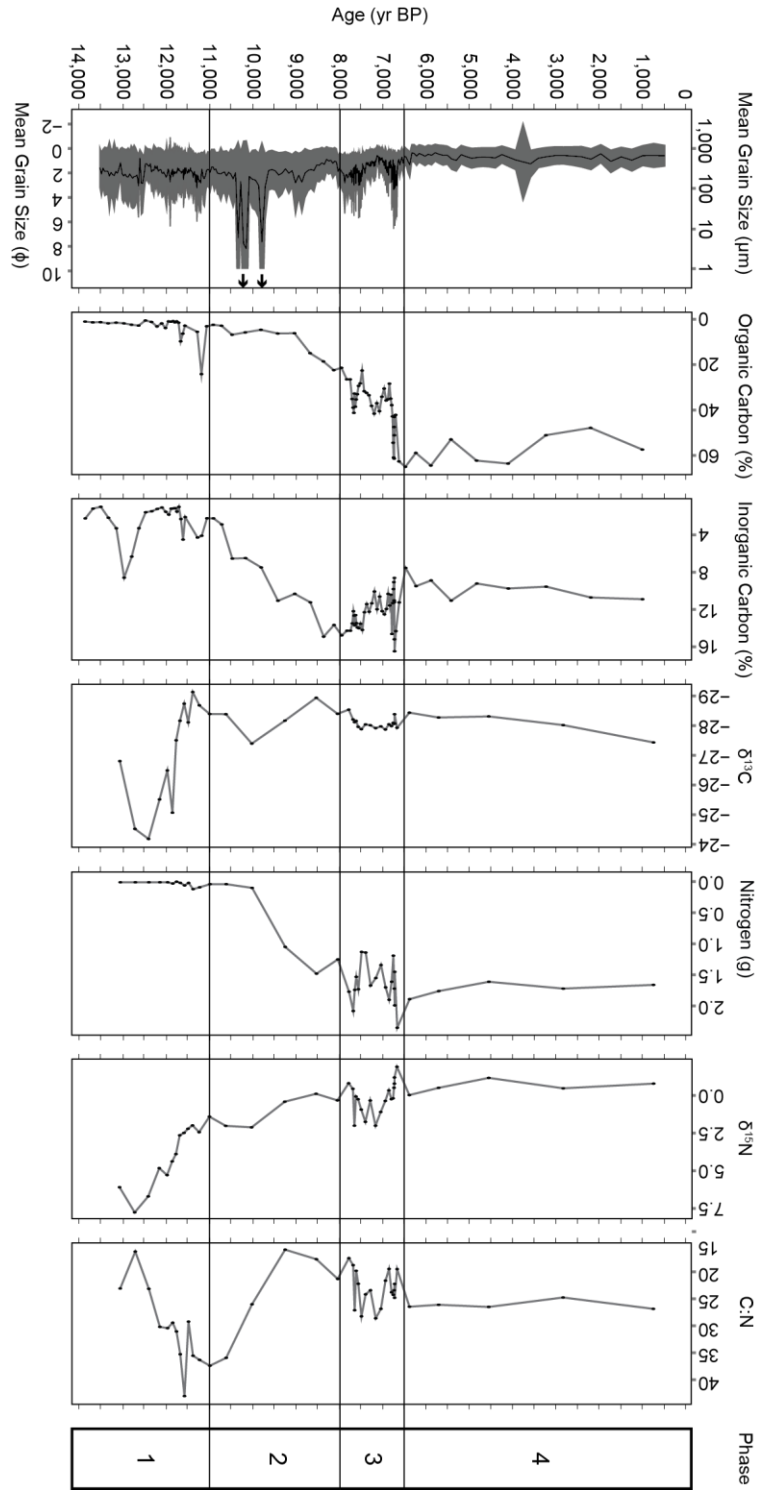

Figure 3.5: Summary diagram of mean grain size, LOI and geochemical data for LSS Core IV. The grey ribbon on the mean grain size data represents within-sample standard deviation in ϕ. Data is divided into different phases using black lines with corresponding phases shown on the right.

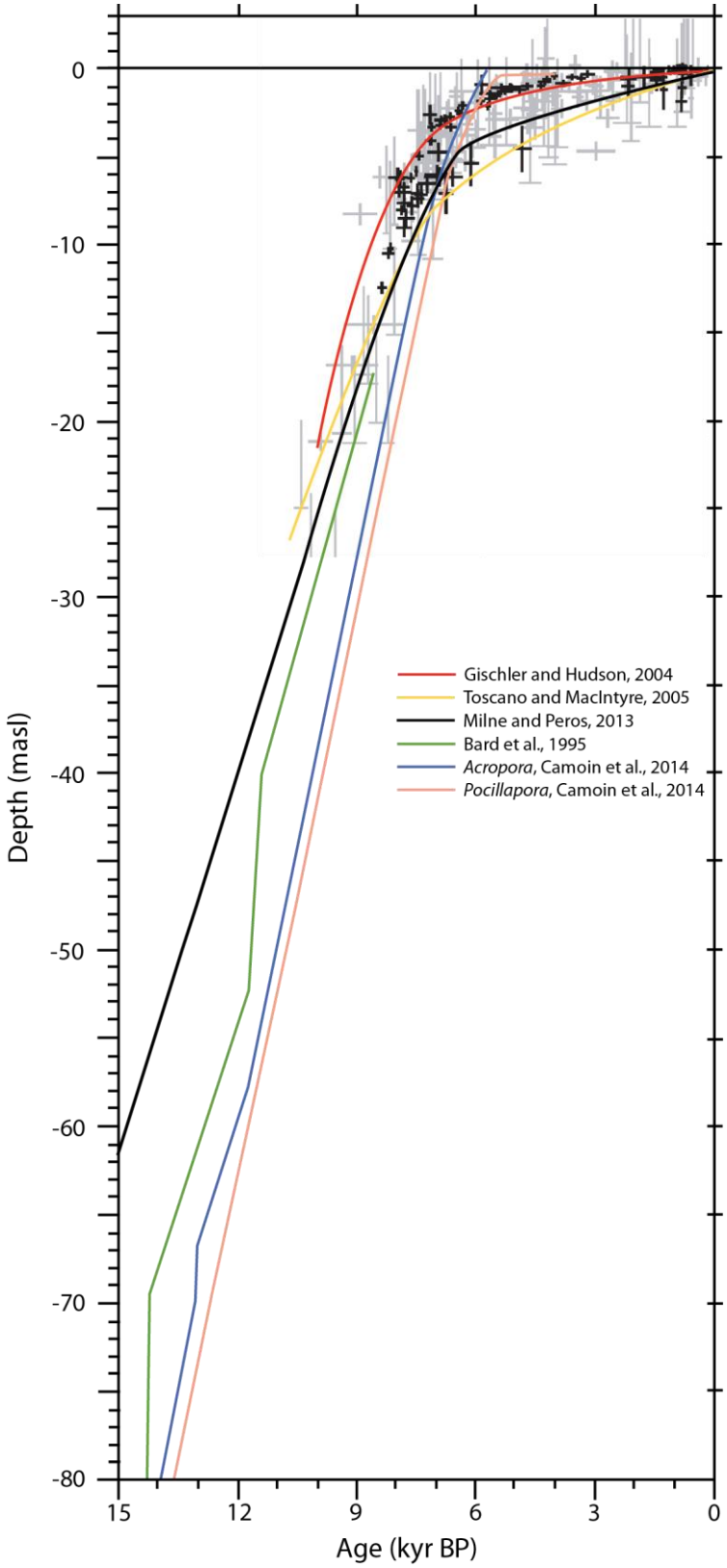

Figure 3.6: Sea level curves and coral growth data for the Caribbean. Data points on the graph are reproduced from the corrected dataset of Milne and Peros (2013). Crosses represent peat deposits with vertical bars representing the range of sea level for each sample point and the horizontal bars representing age related error. Inverted "T"s represent coral sea level points with the lower limit representing minimum sea level and horizontal bars representing age related error.

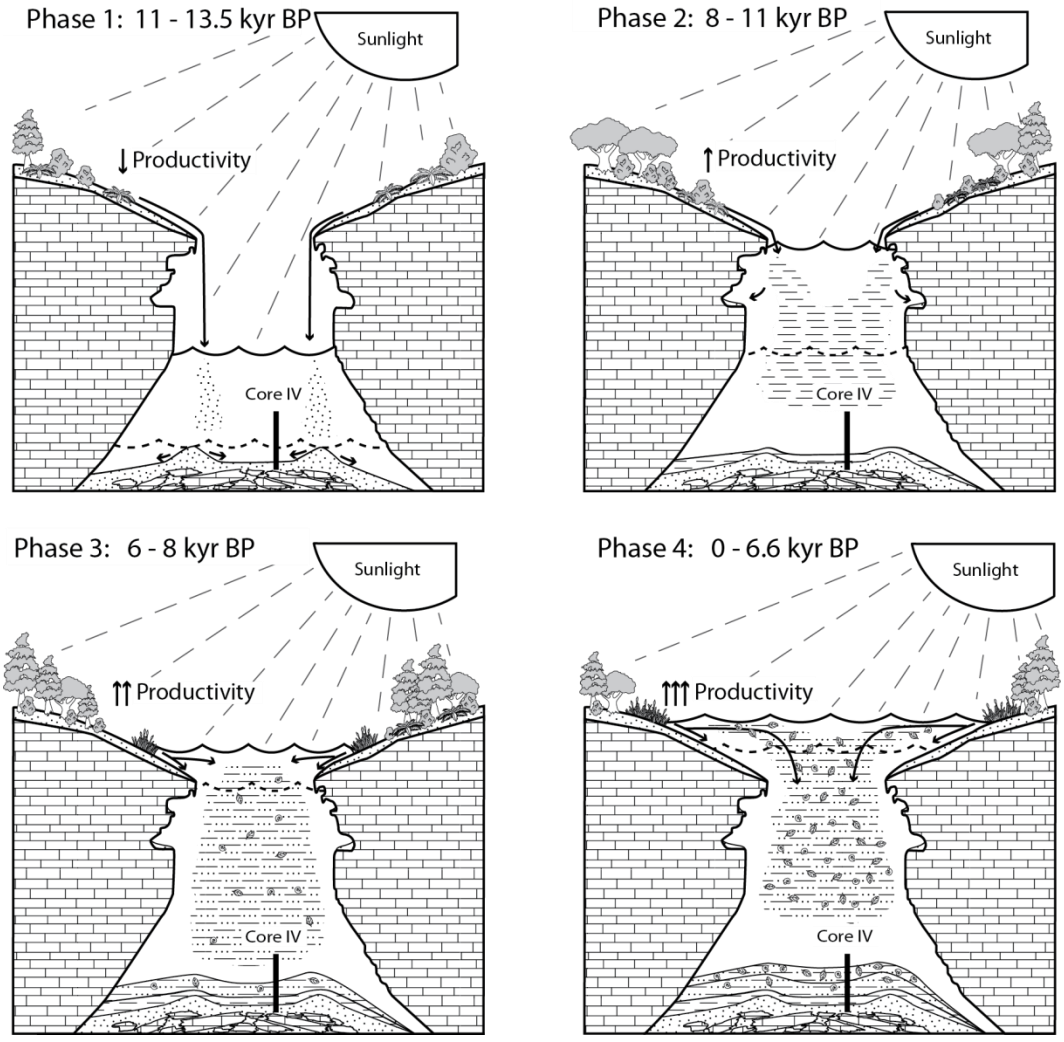

Figure 3.7: Depositional model for LSS. See discussion for more details.

CHAPTER 3 TABLES

Table 3.1: Radiocarbon results from LSS core IV. Beta Analystic results represents dates taken in 1990 (Sample ID 42291, 42292) and 2009. DirectAMS dates were generated in 2013.

Sample ID	Core Drive number	Depth in Drive (cm)	Absolute Depth (cm)	Material Dated	$\delta^{13}C$	Conventional ^{14}C age (yr BP)	Calibrated ^{14}C Age (2σ)
DirectAMS							
D-AMS 005598	1	9	9	Wood	-25.4	2935 ± 28	2996 - 3171
D-AMS 005599	1	45	45	Bulk OM	-27	6811 ± 36	7587 - 7691
D-AMS 005600	2	21	127	Bulk OM	-33.2	5747 ± 34	6453 - 6459
D-AMS 005601	3	17	239	Bulk OM	-27.2	6058 ± 34	6829 - 7000
D-AMS 0055607	3	87	307	Bulk OM	-35.6	6379 ± 36	7256 - 7341
D-AMS 005602	4	17	357	Bulk OM	-31.4	6700 ± 41	7491 - 7624
D-AMS 0055603	4	67	407	Bulk OM	-25.9	6883 ± 32	7662 - 7791
D-AMS 0055604	4	113	453	Wood	-29.5	7044 ± 33	7824 - 7950
D-AMS 0055605	5	19	479	Wood	-25.7	7407 ± 34	8174 - 8327
D-AMS 0055606	6	3	567	Bulk OM	-26.6	9631 ± 37	10787 - 10974
Beta Analytics							
254412	1	82.5	82.5	Twig	-27.9	5720 ± 40	6422 - 6573
254413	2	75.5	181	Twig	-28.4	6190 ± 40	6976 - 7177
254414	3	45	268	Twig	-28.4	7360 ± 40	8041 - 8222
254415	5	70	530	Twig	-24.7	9600 ± 50	10758 - 11157
254416	6	73.5	637	Walnut	-27.5	9980 ± 50	11254 - 11629
42291	6	100	667	Wood		10240 ± 130	11402 - 12421
254417	7	28	707	Charred wood	-28.2	10520 ± 50	12379 - 12615
42292	7	56	735	Charcoal		10210 ± 80	11603 - 12221
254418	7	138	817	Plant fragments	-26.7	11570 ± 60	13279 - 13596

CHAPTER 4

4.1 SUMMARY AND CONCLUSIONS

To increase the efficiency and accuracy of paleoclimate reconstructions in coastal systems, new methods and environments where examined. It is imperative that coastal systems can be used as reliable source of paleoclimate information if Caribbean climate is to be further understood. Developing our understanding of the factors influencing Caribbean climate will ultimately lead to a better understanding of global climate change.

4.2 ADDRESSING THE CENTRAL RESEARCH QUESTIONS

4.2.1 Is XRF a viable source of paleoclimate information?

Core scanning XRF has been useful in the generation of climate data from deep basin and lacustrine records in the past. These systems are ideal for examination with XRF as their stability ensures any shift observed in the trace element record is due solely to external influence. The lack of application of this technique to coastal environments is undoubtedly due to their ephemeral nature. The example of core scanning XRF data from two Cuba lagoons recording a regional signal of decreased precipitation during the Late Holocene suggests that precipitation and possibly other climate signals can be inferred using trace element abundances derived from XRF. In order to increase the confidence of climate inferences recorded in trace element data additional proxies are needed. In this case, foraminifera proved invaluable both recording a similar climate signal, and providing evidence of a relatively stable basin. Foraminifera occupy most coastal environments from marsh to deep basin. The predominance of foraminifera in many coastal environments marsh to shelf, and the relative ease of analyzing XRF data offers a powerful method for the quick, accurate generation of paleoenvirnmental data in coastal settings. Though this study focused on amounts of precipitation inferred from Fe, Ti and K, other trace elements may be of use in coastal environments whose applications range from sediment provenance studies to establishing high-resolution paleo-hurricane records. If XRF is to be reliably used in littoral environments, more studies generating baseline information for comparison with coastal data are needed as well as studies such as this one that correlate multiple proxies to XRF data in order to examine the efficacy of XRF as a recorded of climate signals.

4.2.2 What are the major controls on sedimentation within sinkholes?

Sinkholes are becoming an increasingly important source of paleoclimate information in coastal systems. If sinkholes are to be considered a reliable source of paleoclimate information, there needs to be a more thorough understanding of

the variables influencing sedimentation within sinkholes. Previous work suggested sea level rise was the dominant control on environmental change within sinkholes, however, recent studies suggest the morphology surrounding the sinkhole, and of the sinkhole itself, is similarly important. In Chapter 3 of this dissertation, the sedimentary history of Little Salt Spring (LSS), a sinkhole with distinct morphology, was examined for paleoenvironmental reconstruction. In the case of LSS sea level rise controlled the water level within the sinkhole and the interaction between water and sinkhole morphology altered the sedimentation and productivity within the sinkhole. Climate is thought to have a more subtle influence on sedimentology of the sinkhole. Regional trends in climate altered the sedimentology of the sinkhole only during periods of stable sedimentation. Though there was some evidence of climate interaction near the start of the record, the predominance of redeposited sediment made uncertain the timing of these possible events. This study shows that, although sinkholes may contain long sedimentary records, caution must be used when interpreting the paleoclimate data. Sedimentary evidence from LSS shows that, although the sinkholes may record climate signals from Early Holocene, the strongest climate signals are recent recorded when sinkhole sedimentation is predominantly allocthonous.